Environmental Technology & Innovation 39 (2025) 104272

Contents lists available at ScienceDirect

Environmental Technology & Innovation

journal homepage: www.elsevier.com/locate/eti

Sustainable nexus for treating acid mine drainage: How does bio-alkali matrix impact acidity neutralization and heavy metal removal?

Cong Peng [a], Li Zeng [a,b,*], Yonghong Liu [c], Zhenyu Zhang [a], Jiayi Tang [a], Zhenghua Liu [d], Zhaoyue Yang [d], Huaqun Yin [d], I.A. Ibrahim [e], Ke Zhang [f], Zhendong Yang [a,b,*]

[a] School of Architecture and Civil Engineering, Chengdu University, Chengdu, Sichuan 610106, China
[b] Sichuan Provincial Engineering Research Center of City Solid Waste Energy and Building Materials Conversion and Utilization Technology, Chengdu, Sichuan 610106, China
[c] State Key Laboratory of Desert and Oasis Ecology, Key Laboratory of Ecological Safety and Sustainable Development in Arid Lands, Xinjiang Institute of Ecology and Geography, Chinese Academy of Sciences, Urumqi 830011, China
[d] School of Minerals Processing and Bioengineering, Central South University, Changsha, Hunan 410083, China
[e] Central Metallurgical Research and Development Institute, Cairo 11421, Egypt
[f] CHINA MCC5 GROUP CORP.LTD., Chengdu, Sichuan 610000, China

ARTICLE INFO

Keywords:
Acid mine drainage
Bio-alkali matrix
Heavy metal removal
Neutralization
Sustainable remediation

ABSTRACT

Acid mine drainage (AMD), characterized by high acidity and elevated concentrations of heavy metals, poses a persistent threat to ecological systems. Conventional neutralizers (NaOH, Na_2CO_3, $Ca(OH)_2$) raise pH effectively but generate large sludge volumes and incur high operating costs. Here, three urease-positive microbial consortia, enriched from soil and municipal activated sludge, were cultivated with urea to produce bio-alkali matrices (BAM-A/B/C, final pH 9.3). Abundant $–CONH_2$, $–NH_2$, –OH, and –COOH groups capable of chelating metal ions were found in BAM, suggesting alkaline buffering is complemented by ligand-mediated metal sequestration. When each BAM was mixed with AMD at a 3:10 vol ratio, the effluent pH stabilized at 7 and removal efficiencies reached ~100 % for Al, Fe, Cr, Cd; > 90 % for As, V, Co, Ni; 79–80 % for Cu; and 60 – 62 % for Mn. Geochemical analysis identified Fe/Al hydroxysulfates and organo-metal complexes as dominant precipitates. A full cost comparison showed BAM-A lowered treatment expenses to 35.5 RMB per m^3, which is 12 % below NaOH and 26 % below $Ca(OH)_2$, while reducing sludge generation. Coupling BAM with sulfate-reducing bacterial systems is advisable to enhance Mn and SO_4^{2-} removal. Overall, BAM provides an economical and environmentally sustainable alternative for AMD neutralization by uniting alkaline buffering with organic complexation.

1. Introduction

Acid Mine Drainage (AMD) is one of the most pervasive environmental problems posed by mining operations worldwide.

* Corresponding authors at: School of Architecture and Civil Engineering, Chengdu University, Chengdu, Sichuan 610106, China.
E-mail addresses: zengli512@cdu.edu.cn (L. Zeng), yangzhendong@cdu.edu.cn (Z. Yang).

https://doi.org/10.1016/j.eti.2025.104272
Received 17 May 2024; Received in revised form 28 April 2025; Accepted 12 May 2025
Available online 15 May 2025
2352-1864/© 2025 The Author(s). Published by Elsevier B.V. This is an open access article under the CC BY license (http://creativecommons.org/licenses/by/4.0/).

Characterized by its low pH (0.5–3.5) and high concentrations of dissolved metals such as Fe, Mn, and Al and heavy metals like Cr, As, and Pb, AMD poses significant risks to aquatic and terrestrial ecosystems around the mining area (Jiao et al., 2023). Even decades after a mine is closed, AMD will remain active, causing severe contamination to nearby groundwater or soil, posing a threat to the surrounding environmental safety and human health (Yang et al., 2024).

The global scale of AMD impact is staggering, with over 20,000 abandoned mines, most of which contribute to AMD production (Rezaie and Anderson, 2020). Particularly, in China, the discharge of AMD has reached an alarming total of 3.6 billion tons annually, accounting for nearly 10 % of the national industrial wastewater volume, whereas only approximately 4.23 % of this wastewater undergoes proper treatment (Wang et al., 2024a). In fact, the treatment of AMD is not without complex and costly challenges. It has been reported that managing AMD in areas heavily impacted by mining operations can cost $32 to $72 billion in regions like North America, with similar financial burdens observed globally (Lottermoser, 2015; Otunola and Mhangara, 2024). Apparently, to mitigate its extensive environmental impact, the persistent nature of AMD demands green and economical management strategies.

Current AMD treatment technologies are broadly categorized into active and passive systems (Zvinowanda and Caliphs, 2023). Active treatments are considered the most efficient (above 90 % metal removal), focusing on neutralizing AMD's acidity and removing metals through the addition of alkaline chemicals such as calcium-based (CaO, $CaCO_3$, $Ca(OH)_2$) and sodium-based (Na_2CO_3, NaOH) alkaline reagents (Carneiro Brandão Pereira et al., 2020). These treatments facilitate the precipitation of metal hydroxides as pH levels increase, separating metal precipitates from the liquid phase. Despite their effectiveness, active treatment requires significant material costs and can have substantial environmental impacts. In practice, calcium-based alkalis, although widely used, often suffer from poor acid-neutralizing persistence and can lead to the extensive precipitation of $CaSO_4$ (Song et al., 2022). This substantially increases the volume of sludge produced, thereby escalating the challenges associated with sludge disposal. On the other hand, sodium-based alkalis, while achieving higher neutralization efficiency and less sludge production, are significantly more expensive, costing 3–15 times more than calcium-based counterparts, rendering them less sustainable for long-term use.

Recent advancements in AMD treatment have focused on developing methods that are both more sustainable and cost-effective. A standout is the bio-alkali matrix (BAM) which utilizes natural buffering and metal-binding capabilities of biologically sourced solution produced through the enzymatic breakdown of urea by urease, resulting in a highly alkaline and organic-rich complex. BAM can be synthesized using high-concentration urea wastewater (9.3–23 g/L), significantly reducing costs and promoting a circular economy (Rose et al., 2015; Yujing et al., 2022). Besides, studies highlight the effectiveness and versatility of BAM: Williamson et al. (2020) found that BAM can elevate pH to between 8.8 and 9.8, significantly improving the leaching efficiency of copper-zinc ores compared to traditional inorganic alkalis; Qin et al. (2021) demonstrated that, when the concentration of urea is 0.15 mol/L, the produced BAM could quickly enhance alkalinity and precipitate $CaCO_3$ crystals, useful in concrete repair; Xuesong et al. (2024) applied the bio-alkali matrix (BAM) to acidic metal-contaminated soils (initial pH = 5) to near-neutral levels and significantly enhancing the carbonate-bound fractions of copper and lead. Furthermore, during the urea decomposition and biomass accumulation in BAM production, a variety of organic metabolites, including amino compounds (alkylamines, amides, fatty amines), organic acids (stearic acid, nucleic acids), and thiol compounds (thioalkanes, thioacids), may enhance the removal of heavy metals. These compounds facilitate this process through mechanisms such as salt formation, bridging coordination, charged adsorption, and coagulative precipitation, thereby strengthening the precipitation and removal of heavy metals (Mei et al., 2025; Ruacho et al., 2022; Wang et al., 2021). Consequently, BAM emerges as a promising alternative to traditional acid-neutralizing agents for AMD treatment.

This study embarks with a definitive purpose: to rigorously evaluate the effectiveness of the bio-alkali in managing AMD. We aim to investigate the (bio)chemical efficacy of BAM in neutralizing acidity of AMD and its capacity to remove heavy metals from the drainage. Specifically, our objectives are: i) To determine the ability of BAM to adjust the pH of AMD and compare its performance with traditional chemical reagents; ii) To quantify the capability of BAM to remove heavy metals from AMD and assess its efficiency against established treatments; iii) To evaluate the cost-effectiveness of BAM in the long-term management of AMD, considering operational and environmental impacts. Through this research, we intend to provide a detailed understanding of BAM's potential as a sustainable pathway in AMD treatment, potentially transforming current practices with a more environmentally and economically viable solution.

2. Materials and methods

2.1. Sample collection

Samples for microbial inoculum were collected as follows: Raw-A from topsoil at Chengdu University, Raw-B from the aerobic tank of a wastewater treatment plant in Kunming, China, and Raw-C from an aerobic tank of another wastewater treatment plant in Chengdu, China. Samples were centrifuged (4000 rpm, 20 min) using a SN-LSC-40 centrifuge (Shanghai Shangpu Instrument Equipment, Co., Ltd.), retaining the sludge for experiments and taking 5 g of each for further analysis. AMD was collected from a decommissioned site in northwest China, following standard water examination guidelines. Chemical characteristics of the AMD are detailed in Table 1.

Table 1
Chemical characteristics of the AMD used for experiments.

pH	Al mg/L	Fe mg/L	As mg/L	Cr mg/L	Cd mg/L	Cu mg/L	Mn mg/L	V mg/L	Co mg/L	Ni mg/L	SO_4^{2-} mg/L
2.3	718.25	1034.32	0.07	5.52	4.93	0.42	77.55	20.55	10.35	15.72	9453

2.2. Urease-producing microbial consortia screening

The screening medium was formulated based on previous study (Khadim et al., 2019). Solution A was prepared by dissolving 1 g peptone, 5 g sodium chloride, and 2 g potassium dihydrogen phosphate in 900 mL deionized water and autoclaved at 121 °C for 25 min using a DSX-30L-I sterilizer (Shanghai Shenan, Co. Ltd.) in a 2-liter flask. After cooling under UV light, Solution B was created by dissolving 1 g glucose and 20 g urea in 100 mL deionized water and filtered through a 0.22 μm PTFE filter. Solution B was then added to cooled Solution A to finalize the liquid culture medium.

Three urease-producing microbial consortia (UPMC), UPMC-A, UPMC-B, and UPMC-C, were initiated by adding 5 g of Raw-A, Raw-B, and Raw-C, respectively, to 250 mL conical flasks containing 100 mL of the prepared medium. The flasks were incubated at 30 °C and 100 rpm in a SHA-CB shaking water bath (Changzhou Surui Co., Ltd). Employing semi-continuous cultivation, fresh medium was replaced with 50 mL of spent medium every 48 h until key indicators (ammonia nitrogen, pH, OD_{600}) stabilized. This process produced Bio-alkali matrix reserve liquids (BAMRL-A, BAMRL-B, BAMRL-C) for subsequent BAM preparation, and metagenomic analysis characterized the microbial communities.

2.3. Bio-alkali matrix preparation

To optimize BAM preparation, a 72-h cultivation trial was performed. BAMRL was inoculated (10 % v/v) into a liquid medium identical to the UPMC-enrichment formulation but without dipotassium hydrogen phosphate and sodium chloride; the resulting solution maintained pH 8.3, indicating that further buffering was unnecessary. The inoculation entailed adding 10 mL of BAMRL to 90 mL of the medium in 250 mL conical flasks, incubated without further supplementation under conditions described in Section 2.2. pH, OD_{600}, and ammonia nitrogen levels were monitored at intervals, concluding at 72 h.

Following the initial trial, BAMRL-A, BAMRL-B, and BAMRL-C were each inoculated into fresh medium at a 10 % v/v ratio to produce BAM-A, BAM-B, and BAM-C respectively. This was performed in triplicate in 250 mL conical flasks, following the same protocol and incubation conditions as the trial. The duration of cultivation required to obtain the final BAM products was determined based on the analysis from the 72-h trial. Additionally, 50 mL samples of each BAM type were stored at −60 °C for future analyses, including the identification of organic components and determination of total organic content.

2.4. AMD neutralization experiment setup

For AMD neutralisation we compared the bio-alkali matrices (BAM, pH = 9.3) with three industry-standard chemical reagents supplied at their customary field strengths: 40 % NaOH, 20 % Na_2CO_3 and 20 % $Ca(OH)_2$. A 40 % NaOH solution delivers the high alkalinity required on site yet remains sufficiently fluid for safe handling (solution pH > 14); a 20 % Na_2CO_3 solution, just below its saturation limit (~22 %), provides a stable carbonate–bicarbonate buffer (pH around 11); and a 20 % $Ca(OH)_2$ solution represents the practical upper limit that avoids rapid crystallisation and pipeline fouling (slurry pH > 14). Each reagent, used at its native concentration, was titrated until the AMD reached pH 7.0, after which dosage volume, sludge mass and overall cost were recorded. This target-driven set mirrors real-world operation and allows a realistic economic comparison between conventional bases and the NH_3/NH_4^+-buffered, ligand-assisted neutralisation offered by BAM.

The experimental setup involved placing 100 mL of AMD in a 250 mL beaker and stirring at 400 rpm using a magnetic stirrer (79–1, Beijing Zhongxing Weiye, Co., Ltd.). Titration was conducted slowly with 20 % Na_2CO_3 and the three BAMs using a 50 mL burette, while 40 % NaOH and 20 % $Ca(OH)_2$ were added in increments of 0.01–0.05 mL using a pipette gun. The pH was monitored in real-time until it reached predetermined targets of 3, 4, 5, 6, and 7. Each pH target was tested in triplicate, allowing the pH to stabilize for 5 min before concluding the titration.

After each titration trial, the pH meter probe (TSP > 95 %, E-201F, INESA Scientific Instrument, Co., Ltd) was replaced to ensure accuracy. Following completion of all trials, the mixture underwent solid-liquid separation using qualitative filter paper. The filtrate was collected, passed through a 0.22 μm filter tip, and stored at 4 °C in 250 mL PVC bottles for future metal and sulphate concentration analyses. The sludge generated during the neutralization experiments was quantified using the gravimetric difference method, following SM 2540 D from the Standard Methods for the Examination of Water and Wastewater (APHA, 23rd edition, 2017). After filtration, the sludge and filter paper were dried at 60 °C for 48 h in a drying oven (DHG-9140A, Shanghai Hongdu Electronic Technology Co., Ltd.) until constant weight, and the dry mass was calculated. The sludge dry mass at pH = 7 was used to estimate sludge disposal costs in the subsequent comprehensive cost analysis. Subsequently, the precipitate was ground in a ceramic mortar, sieved through a 100 mesh screen, and stored in a sealed, dry environment for further analysis.

2.5. Chemical measurements

2.5.1. Ammonia nitrogen concentration

The ammonia nitrogen content was measured using a test kit (LH-YN2N3-100, Beijing Lianhua Yongxing Co., Ltd). A 10 mL sample of diluted water was added to a 10 mL colorimetric tube, followed by 1 mL each of reagents LH-YN3 and LH-YN2. After thorough mixing, the mixture was allowed to react at room temperature for 10 min. The ammonia concentration was then read directly at 420 nm using a multiparameter water quality meter (LH-M600, Beijing Lianhua Yongxing, Co., Ltd).

2.5.2. OD_{600} determination

Optical density at 600 nm was measured using a spectrophotometer (UV2150, UNICOSH, Co., Ltd.). The sample was taken from the supernatant, with fresh liquid medium used as the blank.

2.5.3. Sulfate concentration

Sulfate concentrations were measured using a barium chromate method. 5 mL sample was digested with 0.25 mL 2.5 mol/L HCl (110 °C, 15 min) in a LH-1220 digester (Beijing Lianhua Yongxing, Co., Ltd.), followed by 0.25 mL barium chromate. After 10 more minutes of digestion and cooling, 0.5 mL of diluted ammonia was added for 5 min. The solution was filtered through a 0.22 μm PTFE filter and absorbance was measured at 420 nm.

2.5.4. Organic content identification

The total organic matter (TOM) was measured using the NY/T 1121.6–2006 method, suitable for samples with up to 15 % organic content. About 0.5 g of sample was reacted with excess acidic potassium dichromate, heated to 170 °C for 5 min, then cooled. The remaining dichromate was titrated with ferrous ammonium sulfate until a color change from blue-green to reddish-brown indicated reaction completion. Organic matter concentration was calculated from the reacted dichromate. The identification process began with drying chloroform extracts using anhydrous sodium sulfate, followed by evaporation under nitrogen. Samples were derivatized with 0.5 mL of BSTFA: TMCS (99:1, Supelco, USA) at 70 °C for 30 min. Analysis was performed on a Shimadzu GC-2010 Plus gas chromatograph coupled to a TQ8040 triple quadrupole mass spectrometer (Thermo Fisher Scientific, Japan), with an ion source temperature of 250 °C. The GC oven temperature increased from 100 °C (3 min) to 300 °C (5 min) at 8 °C/min. Metabolites were identified using the CAS mass spectral database, with spectra obtained at 70 eV in electron-impact mode.

2.5.5. Metal determination

Metal concentrations were quantified using an iCAP RQ ICP-MS (Thermo Fisher Scientific, Japan). Calibration involved mixed metal standards (0–100 μg/L). Precision was established by measuring a 2 % nitric acid blank ten times, with detection limits set at 3–10 times the standard deviation. Sample preparation included acidifying 4 mL of filtered sample (0.45 μm) with 1 mL of 1 % HNO_3 and dilution for analysis. XRD analysis of sediments was performed (Panalytical, Netherlands) using a copper anode, Kα radiation, and graphite monochromator, scanning from 3° to 80° at 0.02° steps, 0.5 s per step, at 40 kV and 40 mA.

2.6. DNA extraction and sequencing

For the genomic DNA extraction, samples were filtered through a 0.22-μm polyethersulfone membrane (PALL, USA) and the filter was cut into 0.2 cm^2 sections. DNA was then isolated using the E.Z.N.A.® Stool DNA Kit (Omega, USA). Libraries were prepared with the TruSeq Nano DNA LT Library Preparation Kit and sequencing was performed on an Illumina NovaSeq™ 6000 system (LC-Bio Technology, Co., Ltd) with 2 × 150 bp paired-end reads. Data processing included adapter removal with cutadapt v1.9 and subsequent bioinformatics analysis.

2.7. Data processing

Experimental data visualization was performed using Origin2021; Bioinformatic data analysis utilized OECloud tools; XRD phase data was analyzed with JADE6 and visualized in Origin2021. Urease efficiency (Eq. (1)), neutralization (Eq. (2)) and removal (Eq. (3)) efficiencies of various reagents on AMD were calculated. Cost calculations for AMD treatment incorporated total and sub-costs related to water treatment volumes (Eq. (4)). To extrapolate the experimental results to engineering applications, a scaling-up approach was employed for the economic evaluation (Esteban-Gutiérrez et al., 2018; Koskue et al., 2022). All the foundational data were based on the neutralization of AMD to pH = 7.

$$SUD = \frac{AP}{[OD_{600}] \times \mathrm{t}} \tag{1}$$

$$K\mathrm{n} = \frac{\mathrm{d}V\mathrm{n}}{\mathrm{dn}} \tag{2}$$

$$\mathrm{RE} = 1 - \frac{C_{\mathrm{i}}}{\frac{C_0 \times V_{AMD}}{V_{AMD} + V_{\mathrm{Reagent}}}} \times 100\% \tag{3}$$

$$\mathrm{TC} = \sum_{\mathrm{i}=1}^{\mathrm{n}} V_{\mathrm{Treatment}} X_{\mathrm{i}} \tag{4}$$

Eq. (1): The specific urea degradation (SUD) rate quantifies ammonium production per unit of OD_{600} over time (t), with SUD expressed in g L^{-1} h^{-1}, ammonium production (AP) in g L^{-1}, and time (t) in hours (h). Eq. (2): The constant (K_n) signifies the rate of pretreatment at a specified pH, with (dV_n) representing the infinitesimal volume of reagent consumed, and (d_n) the infinitesimal change in pH. The volume (V_n) is measured in milliliters (mL). Eq. (3): The removal efficiency (RE) measures the reduction of metal

elements or sulfate ions (SO_4^{2-}) from AMD when treated to pH = 7. Initial concentration (C_i) and concentration after treatment (C_0) are measured in mg/L. The volumes of AMD (V_{AMD}) and reagent ($V_{Reagent}$) are in liters (L). Eq. (4): The total cost (TC) encompasses all expenses for treating each cubic meter of AMD to pH = 7, expressed in RMB/m^3. It includes the volume of treatment ($V_{Treatment}$) in m^3 and the cost components (X_i), including reagent, sludge disposal and water expenses (Data obtained from the Chinese National Development and Reform Commission), in RMB/m^3.

3. Results and discussion

3.1. Optimization of UPMC growth and BAM preparation timing

To select a consortium with urease metabolic activities, semi-continuous cultivation supplied consistent urea and nutrients, providing microbes with ample substrates for steady physiological and biochemical progression until stable endpoints were reached. Moreover, to elucidate the growth dynamics of UPMC in the medium and determine the duration for BAM preparation, we conducted a 72-h continuous cultivation trial. The cultivation cycles were named with Ci, where i refers to the cycle number. After determining the optimal cultivation time of 72 h, we explored how the cultivation temperature affects the final pH value of BAM.

Stability in OD_{600}, ammonia nitrogen, and pH readings, illustrated in Fig. 1A–C, during C5-C7, informed the conclusion of cultivation after C7, resulting in the generation of UPMC liquid. Initially, the culture system presented a mild acidity at C0 due to the release of H^+ from dipotassium hydrogen phosphate in the culture medium. During the C1, the pH of the liquid medium approached 9.3, indicative of urea breakdown by urease-producing microbes, as seen in the production of ammonia, supporting the findings of Diez-Marulanda and Brandao (2023). The ammonia, highly soluble in water, dissociated to yield OH^-, contributing to the pH increase. This pH fluctuation aligns with patterns reported in other urease-producing microbe selection studies (Jalilvand et al., 2019; Jiang et al., 2016). Biomass density in the UPMC-A, UPMC-B, and UPMC-C media surged during the C1-C2 initiation phase, likely linked to the rich microbial community in the initial samples and externally supplied nutrients, which facilitated robust microbial proliferation in the early stages. Additionally, the ammonium from urea decomposition likely fueled ATP production, hence boosting metabolism and enzyme activity (Hamzah et al., 2013; Mempin1 et al., 2013), contributing to the rapid microbial growth observed, particularly for UPMC-A, where OD_{600} reached 2.0.

As semi-continuous cultivation progressed, a decline in OD_{600} values from C3 suggested microbial mortality. We speculate this was due to high concentrations of free ammonia permeating microbial cell membranes, disrupting proton balance, and altering

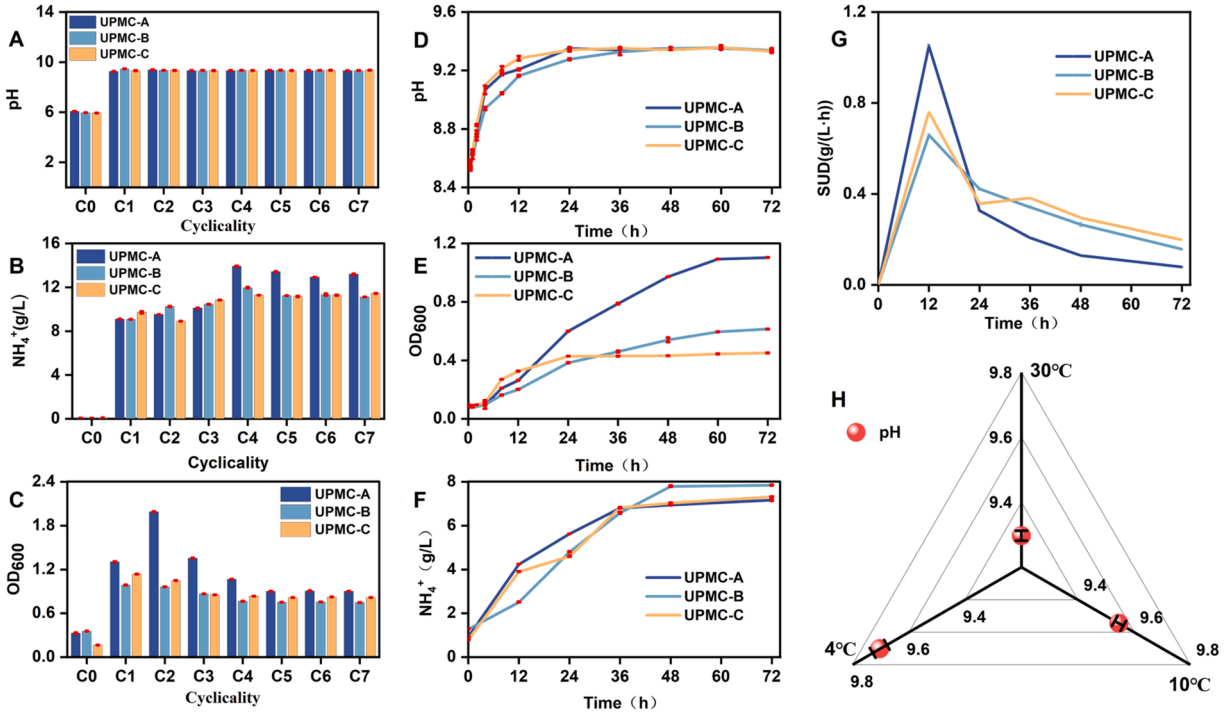

Fig. 1. Dynamic profiles of microbial cultivation and activity in UPMC. A–C show the semi-continuous screening process of UPMC, monitoring pH, OD_{600}, and NH_4^+ across seven cycles (C1-C7). D-G shows the dynamic profiles of pH, OD_{600}, NH_4^+, and SUD over a 72-h continuous cultivation period following inoculation with 10 % (v/v) UPMC. The SUD values, where higher readings reflect greater urea decomposition efficiency, are emphasized to illustrate enzymatic activity across the cultivation timeline. F shows the effect of temperature on pH endpoint values of BAM set at 30 °C, 10 °C, and 4 °C.

intracellular pH, diminishing enzymatic efficiency and increasing energy requirements for cell maintenance (Palakodeti et al., 2021). Additionally, an alkaline environment, while inhibiting microbial proliferation (Fan et al., 2020), is generally hostile to most microbes, which may elucidate the observed microbial die-off at the elevated ammonia nitrogen levels and pH of 9.3. This is in concordance with similar findings from a previous study regarding the influence of pH and ammonia nitrogen on biomass (Yang et al., 2020). In later cycles, although OD_{600} fluctuated marginally around 1.0, ammonia nitrogen concentrations remained above 10 g/L at pH 9.3. Bacteria following the urea degradation pathway typically meet longevity, non-pathogenicity, and survival in alkaline conditions criteria (Marín et al., 2021), confirming the presence of urease metabolic pathway microorganisms in all three samples. Elmi et al.(2022) subjected four purified strains (*Sporosarcina pasteurii*, *Lysinibacillus boronitolerance*, *Bacillus spp.*) to stress tests (pH, temperature, NaCl concentration), observing inhibition at pH 9. However, our UPMC maintained urea degradation capabilities at pH 9.3, suggesting a greater alkaline tolerance compared to single colonies.

Pure cultures of urease-producing bacteria exhibit significant limitations such as difficulty in maintaining enzyme activity, poor environmental adaptability, and high costs (W. H. Liu et al., 2022). Therefore, screening mixed bacterial cultures can mitigate these drawbacks. The initial materials for UPMC were sourced from soil or aerobic sludge from municipal wastewater treatment plants. The residues of plants and animals in the soil provide energy substances for microbial activities, making soil a treasure trove of microbial diversity. Many researchers have successfully isolated urease-producing bacteria from soil using urea media (Alizadeh et al., 2017; Gupta et al., 2022). Similarly, species of urease-producing bacteria persist in the nutrient-rich sludge of wastewater treatment plants, with numerous successful isolations reported from these sources (Newton et al., 2022; Xu et al., 2017a; Yang et al., 2020). This discussion highlights the broad range of sources for urease-producing bacteria. In our work, the successful selection of urease-producing bacteria was indicated by a rapid increase in pH and ammonia nitrogen within a short period (2 days), demonstrating the short screening cycle for these bacteria.

Fig. 1D—G detail the pattern of indicator changes during the 72-h continuous cultivation. For Fig. 1D, pH significantly changed over time, with an initial weak alkalinity due to the addition of BAMRL (pH 9.3), followed by a rapid ascent to pH 9.3 within 0–24 h for all three samples, and stability at this pH from 25 to 72 h, mirroring the end-point pH pattern in the continuous UPMC screening. Fig. 1D illustrates the change in OD_{600} over time for bacterial cultures. In the 0–24 h period, the OD_{600} values for UPMC-B/C rapidly increased, followed by a slower growth rate from 25 to 72 h, which then plateaued. This pattern aligns with the semi-continuous screening process of UPMC, and it is hypothesized that this is mainly due to pH elevation and toxicity inhibition of bacterial growth caused by an increase in NH_4^+ concentration resulting from urea decomposition. However, UPMC-A exhibited a different pattern, with continuous growth in OD_{600} from 0 to 60 h before plateauing from 61 to 72 h. The reason for this anomaly is related to the specific bacterial communities within UPMC, which will be further elaborated in Section 3.3 during the microbial community analysis. In the 0–48 h interval, the concentration of NH_4^+ increased over time with a significant slope in the curve. Despite the growth inhibition observed in UPMC-B/C after 24 h, urea concentration continued to increase between 25 and 48 h, indicating that urea decomposition in UPMC-B/C was not limited by bacterial growth inhibition. The peak NH_4^+ concentration for UPMC-A/B/C was reached at 48 h, with little change observed from 48 to 72 h, and the concentrations were similar across all variants, suggesting that the final NH_4^+ concentration is more dependent on the substrate urea concentration rather than bacterial OD_{600}. Fig. 1G presents the curve for the change in urea decomposition efficiency over time within the bio-amino matrix. The pattern observed was an initial increase, followed by a decrease, and finally stabilization, similar to findings from a previous study (Ghezelbash and Haddadi, 2018). Notably, at 12 h, UPMC-A exhibited peak urea decomposition efficiency (SUD = 1.05). Additionally, despite the lower OD_{600} values at this time compared to other intervals, the SUD value was the highest, indicating that UPMC can begin functioning effectively in a short timeframe, which is beneficial for accelerating the preparation process of BAM.

Fig. 1H presents the results exploring the impact of temperature on the final pH values of BAM preparations, cultivated over 48 h. The final pH values of the three different UPMC variants were essentially the same at any given temperature, indicating a commonality in the endpoint pH values of the three types of BAM at the same temperature. The overall trend showed that as the temperature decreased, the pH endpoint values increased: at 30 °C, the pH was 9.30; at 10 °C, it was 9.55; and at 4 °C, it reached 9.73. According to Henry's Law, the decrease in temperature reduces the kinetic energy of gas molecules, making them more likely to be captured by and remain in the liquid, thus increasing the amount of ammonia dissolved in the liquid (Sander, 2015). In summary, UPMC has a wide range of bacterial sources, which can be rapidly selected from soil and nutrient-rich sludge using urea media, and these sources demonstrate a capacity to tolerate weakly alkaline conditions and high ammonia concentrations. The specific advantageous communities will be detailed in Section 3.3 during the analysis of community structure. The endpoint pH value of UPMC is influenced by both temperature and the concentration of urea in the substrate. Therefore, the broad source of urease-producing bacteria and the short screening time are valuable for the application of BAM. Minor fluctuations in SUD values at 48 h across all UPMC samples highlight the critical 48-h incubation period for obtaining BAM using BAMRL inoculation. This part produced UPMC liquid as a microbial consortium harboring urease metabolic activities, and the 72-h trial suggested a 48-h BAM preparation period, establishing a timeline for BAM production. When the temperature is lowered, the BAM obtained after a 48-h cultivation exhibits a higher endpoint pH value, which can effectively reduce the volume of BAM used for neutralizing pH in AMD wastewater. This also serves as important guidance for optimizing the culture medium in different temperature usage scenarios.

3.2. Chemical and functional characterization of BAM

BAM was synthesized by inoculating a 10 % volume of BAMRL into a liquid culture medium, subsequently cultured for 48 h. The resultant BAM variants, namely BAM-A, BAM-B, and BAM-C, achieved a consistent pH of 9.3, with OD_{600} values of 0.45, 0.55, and 0.91, respectively. To elucidate the composition of organic metabolites within BAM, GC-MS analysis was employed, focusing on

organic substances equipped with metal ion chelating functional groups. Concurrently, the TOM concentration was determined. The results, as presented in Table 2, indicate a compositional consistency between BAM-B and BAM-C, diverging from BAM-A, with TOM values ranging between 0.44 and 0.45 g/L across the three BAM types (Data not shown). This suggests a significant organic content within BAM, capable of providing a plethora of reactive functional groups.

In-depth examination through the Chemical Database of the Chinese Academy of Sciences (CSDB) highlighted that functional groups such as -$CONH_2$, -NH_2, -OH, and -COOH are adept at forming stable complexes with heavy metal ions through coordination interactions, attributed to the lone electron pairs on nitrogen and oxygen atoms within these groups (Biswas and Biswas, 2023). -NH_2 groups, upon protonation, acquire a positive charge, conferring an attraction to negatively charged heavy metal ions, while -OH groups can also partake in protonation (Jiang et al., 2023; Qiu et al., 2022). Both -$CONH_2$ and -COOH are prone to protonation, potentially releasing H^+ ions in acidic metal-bearing wastewaters, and forming stable chelates with heavy metal ions, existing as coordination complexes (Kanmani et al., 2017; Lu et al., 2020; Turingan et al., 2021). The propensity of these functional groups to neutralize acidic liquids through protonation, although potentially sacrificing ligand capacity, is a critical property for wastewater treatment applications. Notably, BAM-A identified the presence of Cyclo(glycylprolyl), an alkaline substance capable of neutralizing H^+ in acidic environments.

Relevant studies have leveraged active functional groups for heavy metal chelation removal. Turingan et al. (2021) utilized substances with -NH_2 and -OH groups for AMD treatment. Sun et al. (2020) reported evident metal removal from electroplating wastewater using modified chitosan, featuring -OH and -NH_2 functional groups. Applications in heavy metal adsorption from wastewater with chelating resins have highlighted carboxyl and amine groups as two of the most effective functional groups for metal removal from aqueous solutions (Emik, 2014). Lopez et al. (2018) achieved over 90 % interception efficiency for metals (Fe^{2+}, Zn^{2+}, Cu^{2+}) using a composite material with a semi-aromatic polyamide active layer containing carboxyl (-COOH) and amine (-NH_2) groups. These findings corroborate the feasibility of removing metal ions from wastewater via chelation with functional groups. These findings affirm that chelation between metal ions and functional groups is a viable route for metal removal from wastewater. With BAM enriched in active functional groups and Cyclo(glycylprolyl), it theoretically possesses the dual capability to neutralize the acidity of AMD and facilitate metal ion removal through chelation, bolstering its potential application in AMD treatment. In fact, the ability of functional groups like -$CONH_2$, -NH_2, -OH, and -COOH to chelate heavy metals is primarily due to the presence of lone pairs on nitrogen and oxygen atoms, which can form coordination bonds with metal ions. This interaction is essential for the stability of metal complexes. The spatial arrangement of these atoms and the flexibility of the molecule can affect the accessibility of the lone pairs to participate in metal binding. This suggests a more detailed exploration into the electronic structures of these groups could enhance our understanding of their chelation mechanisms. Analyzing the electron density and spatial orientation might provide insights into how these groups interact with different metal ions, potentially influencing the design of more efficient chelating agents.

Table 2
Identification of organic compounds in BAM. Cells shaded in light green indicate the presence of a compound in a particular BAM variant, while cells shaded in light red denote its absence.

Organic matter	CAS	Chemical formula	Functional group	Ligating atom	Chelation reaction (with M^{2+})	BAM-A	BAM-B/C
Alkanes	/	C_nH_{2n+2} (C=8—20)	/	/	/		
2,2'-(hexadecylazanediyl)diethanol	18924-67-9	$C_{20}H_{43}NO_2$	-NH_2	N	$M^{2+}+RNH_2 \rightarrow M-RNH_2$		
Ethanamine	85404-22-4	$C_4H_{12}CN$	-NH_2	N			
Acetamide	60-35-5	$C_{10}H_{15}NO_3$	-$CONH_2$	N			
N-Methylpropionamide	1187-58-2	C_4H_9NO	-$CONH_2$	N	$M^{2+}+RCONH^2 \rightarrow M-RCONH_2$		
N,N-Diethylformamide	617-84-5	$C_5H_{11}NO$	-$CONH_2$	N			
(Z)-docos-1,3-enamide	112-84-5	$C_{22}H_{43}NO$	-$CONH_2$	N			
2-Methyl-1,3-butanediol	684-84-4	$C_5H_{12}O_2$	-OH	O			
Glycerol	56-81-5	$C_3H_8O_3$	-OH	O			
1-Monomyristin	75685-84-6	$C_{17}H_{34}O_4$	-OH	O	$M^{2+}+ROH \rightarrow M-ROH$		
1-Monopalmitin	19670-51-0	$C_{19}H_{38}O_4$	-OH	O			
Glycerol monostearate	1188-75-6	$C_{21}H_{42}O_4$	-OH	O			
2-Ethylbutyric acid	88-09-5	$C_4H_3N_3O_4$	-COOH	O	$M^{2+}+RCOOH \rightarrow M-RCOOH$		
3-Oxopentanoic acid	1821-02-9	$C_5H_8O_3$	-COOH	O			
Cyclo(glycylprolyl)	19179-12-5	$C_7H_{10}N_2O_2$	/	/	/		
D-Threonine	632-20-2	$C_4H_9NO_3$	/	/	/		

3.3. Microbial community dynamics and dominant profiles of UPMC

In the quest to enrich a microbial consortium capable of urease metabolism, initial samples were subjected to a selective process using a urea-supplemented liquid culture medium. To investigate the structural changes in the microbial community before and after selection, and to identify dominant microbes within the UPMC, microbial community analysis at different levels was performed on the initial samples and the three UPMC variants.

Fig. 2A shows the dominant microbes at phylum level. In Group A, *Proteobacteria* was the dominant family in Raw-A, which shifted to *Firmicutes* (comprising over 80 %) in UPMC-A after the selection process. This shift is likely attributable to the robust cell walls and endospore production of *Firmicutes*, enhancing their adaptability to alkaline environments (Zhou et al., 2020), and could explain the sustained increase in OD_{600} values for UPMC-A observed during the 72-h continuous cultivation. *Firmicutes* are known to significantly promote carbon cycling and are crucially involved in most carbon metabolism pathways (Pang et al., 2017), and are also significant contributors to the nitrogen cycle (Ospina-Betancourth et al., 2020). In UPMC-B and UPMC-C, *Proteobacteria* remained dominant, a phylum known for its roles in carbon and nitrogen cycles (Jia et al., 2020). Other dominant families across all groups included *Bacteroidota* and *Actinobacteriota*, with *Bacteroidota* playing a major role in the hydrolysis of organic substances and some *Actinobacteriota* species participating in nitrogen cycling related to urea decomposition (Liu et al., 2023; Thomas et al., 2011).

The microbial diversity within the three UPMC largely displayed simplicity in community assembly, with the functionality of these communities being highly predictable and predominantly determined by the availability of nutrients (Goldford et al., 2018). These bacteria collaboratively participate in carbon and nitrogen cycling, synergistically maintaining the diversity and functional balance of the microbial community. Fig. 2B illustrates the proportional changes at the family level in the bacterial communities before and after selection. Integrative analysis with Fig. 2C, which shows the microbial composition at genus level, reveals that in Group A, *Bacillaceae* (~60 %) and *Planococcaceae* (~20 %) are predominant, with species like *Pseudogracilibacillus* and *Sporosarcina* having the highest representation. Many bacteria within *Bacillaceae* possess urease metabolic pathways and are highly efficient in urea decomposition (Heidari Nonakaran et al., 2015), with reports indicating that *Pseudogracilibacillus* species harbor urease pathways (Dubey et al., 2021).

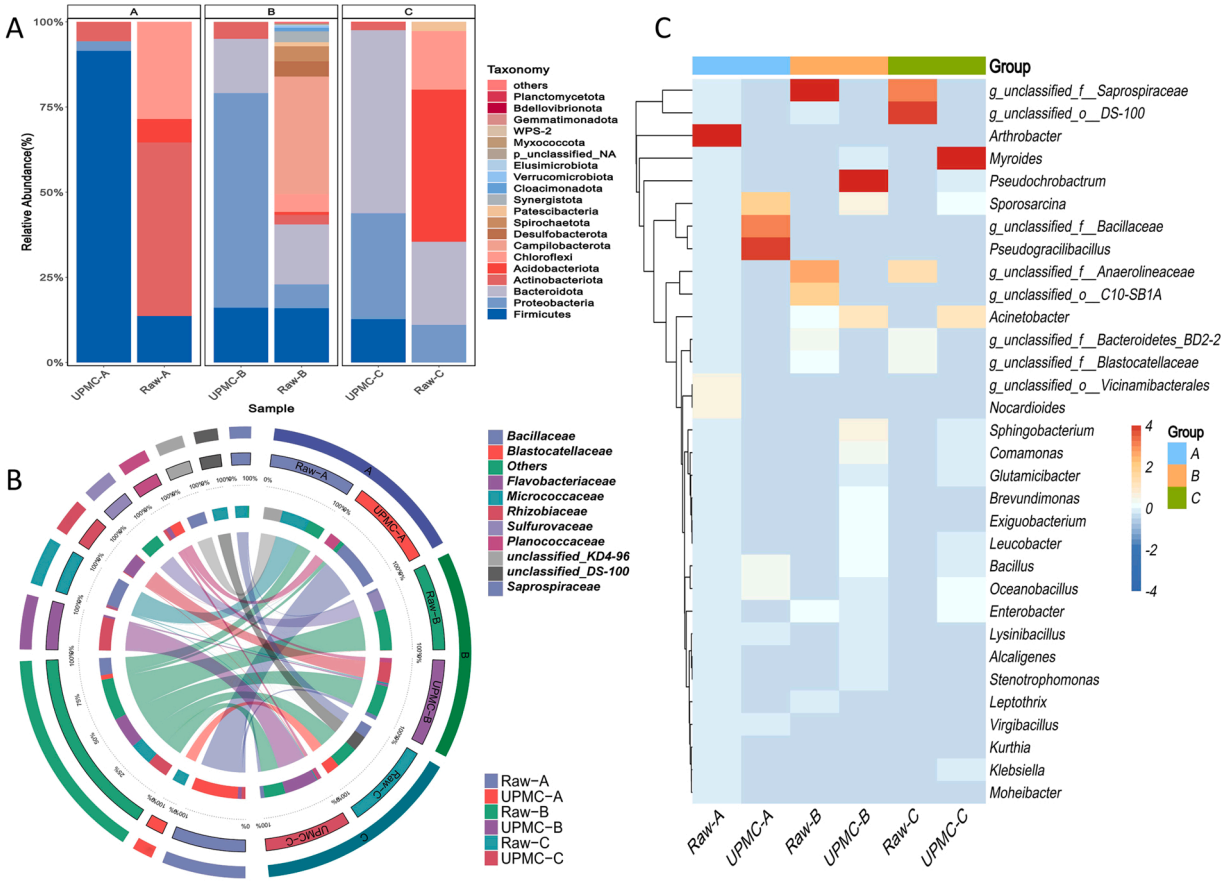

Fig. 2. Comparative analysis of microbial community shifts post-selection process. A shows a cumulative bar chart showing the microbial composition changes at phylum level. B shows a Circos plot that represents microbial composition changes at the family level. C shows a heatmap detailing the microbial composition changes at the genus level; the color gradient from blue to red in the heatmap corresponds to the z-scores, where blue indicates values below the mean and red indicates values above the mean.

Sporosarcina, for instance, secretes urease, facilitating ammonia production from urea decomposition (Ma et al., 2020). These three bacterial species significantly influence the urea decomposition efficiency in UPMC-A. In Group B of Fig. 2C, the characteristic abundance in UPMC-B is *Pseudochrobactrum*, belonging to *Proteobacteria*, with reports of urease pathway presence allowing for urea decomposition (Mao et al., 2015). Other potential contributors in UPMC-B include *Bacillus* and *Sporosarcina*. In Group C, *Flavobacteriaceae* dominates UPMC-C (~70 %), containing key nitrogen cycling microbes (Zhu et al., 2018). Myroides from *Flavobacteriaceae* is the dominant species in UPMC-C, demonstrated to enhance soil enzyme activities when introduced into soils (Wang et al., 2022), and enriching urease content in compost when used in a mixed microbial consortium (Shi et al., 2022). These results indicate that each UPMC hosts a diverse microbial consortium equipped with urease metabolic pathways, illustrating the complexity and specificity of microbial community adaptations and interactions within such engineered environments.

3.4. Geo-chemical transformation of precipitate in BAM treated AMD

To delineate the composition and transformation patterns of precipitates formed when BAM neutralizes AMD to designated pH levels, XRD analysis was carried out for precipitates formed at specific pH levels. XRD patterns, characterized by broad peaks indicative of amorphous materials, were compared with the International Centre for Diffraction Data (ICDD) standards.

We calculated the weighted-profile R-value (Rwp) to assess the phase fit against reference materials (Fig. 3). An Rwp below 10 % generally signifies a reliable match, confirming the accuracy of our results (Toby, 2006). Notably, all Rwp values reported in Fig. 3 were below this threshold, supporting the robustness of our analytical methods. The XRD diagrams revealed consistent changes in peak characteristics across all three BAM variants at specific pH levels, suggesting a systematic transformation in precipitate composition.

Our analysis detected that the dominant peaks for BAM-A-4, BAM-B-4, and BAM-C-4 corresponded with the known peaks of schwertmannite ($Fe_8O_8(OH)_x(SO_4)_y$, with 8-x = y and 1.0 ≤y ≤ 1.75, PDF#47–1775). This alignment, coupled with similar findings in

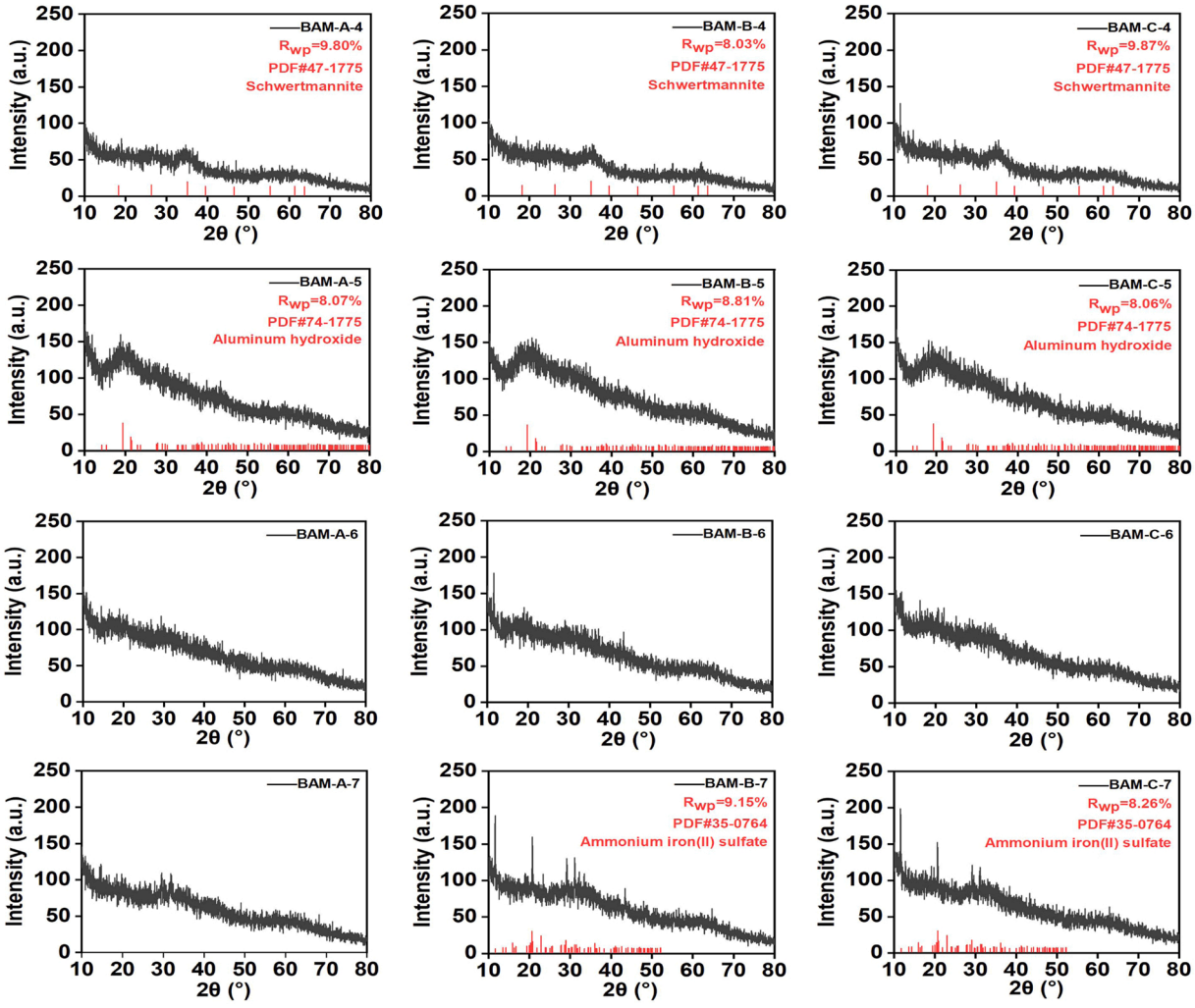

Fig. 3. XRD patterns of precipitates formed where BAM was used to treat AMD to specific pH levels (4, 5, 6, and 7).

other studies (Ding et al., 2022), and the yellowish-brown coloration of the precipitates observed in Fig. 4B, suggests the formation of schwertmannite. The formation mechanism involves BAM addition reducing acidity by consuming H^+ ions and introducing NH_4^+, promoting schwertmannite formation within the optimal pH range of 2.5–4.5 (He et al., 2024). The weaker intensity of the schwertmannite peaks may be due to short mineralization periods or interference from other substances (Paikaray, 2021).

At pH 5, the characteristic peaks of schwertmannite disappeared in samples BAM-A-5, BAM-B-5, and BAM-C-5, aligning with the mineral's stability profile between pH 2.5 and 4.5 (Johnston et al., 2016), and were identified as $Al(OH)_3$ (PDF# 74-1775). At pH 7, the primary peaks in BAM-B-7 and BAM-C-7 closely matched those of $Fe(NH_4)_2{\cdot}(SO_4)_2{\cdot}6H_2O$ (PDF#35–0764), indicating the formation of this complex, absent in BAM-A-7. This detailed characterization of precipitates via XRD provides crucial insights into the transformations occurring as BAM neutralizes AMD to specific pH values, guiding further optimization of BAM application in AMD treatment. The discovery that precipitates such as schwertmannite and $Fe(NH_4)_2{\cdot}(SO_4)_2{\cdot}6H_2O$ can facilitate sulfate removal offers a promising avenue for environmental remediation strategies. Notably, the absence of peaks for other metals in AMD precipitates may be due to their low concentrations. Particularly, they may also form poorly crystalline structures that do not yield distinct XRD signals, and thus are overshadowed by the same but strong amorphous curves produced by large amounts of the main component, particularly schwertmannite.

3.5. *Efficacy of BAM in AMD neutralization and heavy metal removal*

To verify the capability of BAM in neutralizing AMD and removing heavy metals, we conducted titration experiments with three types of BAM (pH = 9.3) on AMD samples. The volume of titrant used and the weight of precipitates formed were meticulously recorded. For comparative purposes, titrations were also performed with traditional neutralizing agents, 40 % NaOH (a strong base), 20 % Na_2CO_3 (a weaker base, pH = 9.9), and 20 % $Ca(OH)_2$. This comparison aimed to highlight differences between BAM and conventional alkaline reagents. Additionally, changes in the color of the AMD solution and the precipitates were observed and recorded as the titration progressed to specific pH levels.

Notably, changes in the turbidity and color of the AMD were documented in Fig. 4A. The initial yellow-brown color, primarily due to the presence of Fe^{3+} in the AMD, shifted across the pH range. At pH 2.3–3, all solutions except those treated with 20 % $Ca(OH)_2$ remained clear, indicating minimal precipitate formation and suggesting that the primary reaction was acid-base neutralization. Conversely, the solution treated with 20 % $Ca(OH)_2$ turned turbid and reddish-brown, likely due to the formation of $Fe(OH)_3$ and $CaSO_4$. As the pH increased from 3 to 6, all solutions predominantly displayed a brownish-yellow hue. At pH 7, except for the 20 % $Ca(OH)_2$ treatment which turned dark green, the 40 % NaOH solution exhibited the deepest greenish-gray, possibly indicating the formation of $Fe(OH)_2$, which appears green in solution. However, the BAM-treated solutions showed lighter shades, suggesting that Fe^{2+} hydroxide formation was not the predominant reaction in BAM, as confirmed by XRD analysis. The precipitate mass produced by all six reagents at pH 3 was minimal; therefore, for consistency in our discussions of precipitate mass, we treat it as zero at pH 3. Fig. 4B demonstrates a consistent pattern in the colors of precipitates generated by the six reagents when treating AMD, with 40 % NaOH and 20 % Na_2CO_3 producing a rust-like color at pH 4, while the colors of the other precipitates varied shades of brownish-yellow.

The results from Fig. 5A and B show that the volume of titrant used and the corresponding changes in neutralization capacity (Kn)

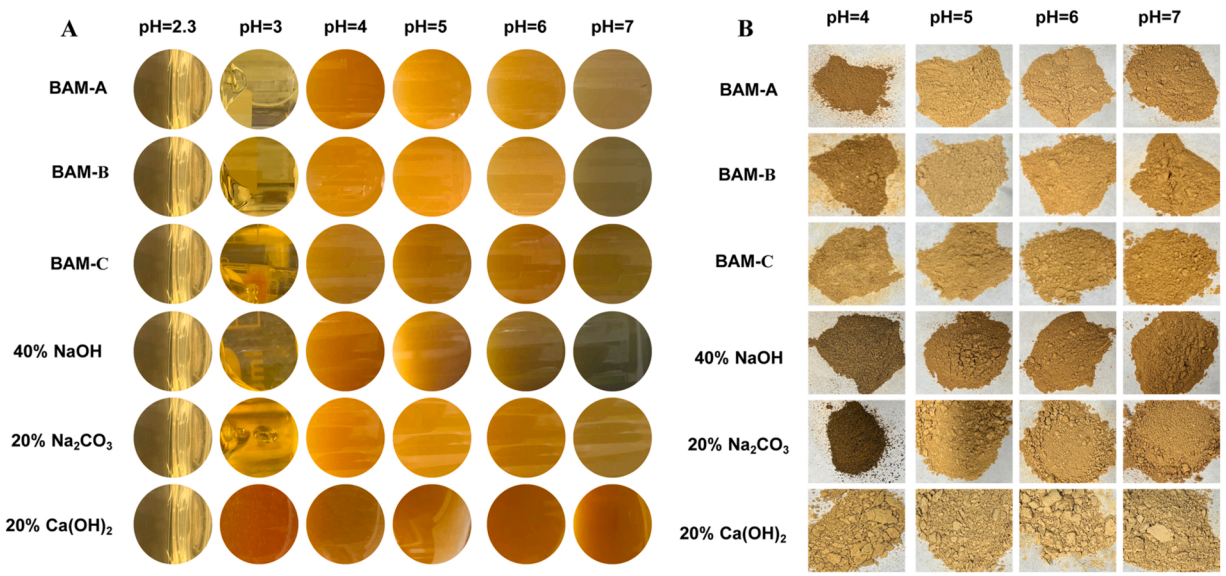

Fig. 4. Visual representation of AMD treatment using various alkaline reagents. The left panel displays the color changes in the liquid phase when the alkaline reagents treat AMD to achieve specific pH levels. The right panel depicts the precipitated materials formed under the same conditions. Notably, at pH 3, minimal precipitate formation occurs, and thus, these results are excluded from the display.

for 40 % NaOH and 20 % $Ca(OH)_2$ followed similar patterns, with these reagents requiring smaller volumes due to their strong alkaline nature, fulfilling the OH- demand of AMD more efficiently. The three types of BAM, along with 20 % Na_2CO_3, required larger volumes to achieve the same neutralization, with 20 % Na_2CO_3 showing the largest volume and lowest efficiency. Theoretically, BAM would need 32 L to neutralize free H^+ without accounting for metal cation interactions. However, experimental titrations demonstrated that only 28–31 mL of BAM was necessary to neutralize AMD to pH 7, suggesting that active functional groups within BAM, through protonation and metal chelation, reduce the overall demand for OH^-, with BAM-A showing the smallest volume requirement. Fig. 5C presents the precipitate formation resulting from titration with six different reagents to designated pH levels in AMD. Notably, the concentrations of Fe and Al in the AMD significantly exceed those of other metals, often by more than tenfold. Consequently, the variations in the precipitate masses of Fe and Al are particularly significant in our analysis. The data reveal diverse pathways for metal removal from AMD, as evidenced by the varying amounts of precipitates produced when the AMD is titrated to specific pH levels with each reagent. At pH 3, the precipitate mass was essentially negligible. Accordingly, for consistency across the study, we consider the precipitate mass at this pH level to be zero.

At each specified pH level (excluding pH 3), 20 % $Ca(OH)_2$ produced the highest amount of precipitate, distinguishing it from the other reagents. At pH 4, the majority of the precipitates consisted of Fe^{3+} (Li and Zhang, 2022). However, the three types of BAM generated a greater mass of precipitates than did 40 % NaOH. This increased precipitate mass is primarily attributed to the BAM inducing the formation of schwertmannite, which incorporates additional SO_4^{2-} into the precipitates. By pH 5, a considerable portion of the precipitates was composed of Al hydroxide (Seo et al., 2017). Additionally, the difference in precipitate mass between the three types of BAM and 40 % NaOH became more pronounced, likely because the BAM facilitated the inclusion of larger molecular weight organic compounds into the precipitates through the chelation of metal ions by active functional groups. By pH 7, the target endpoint for pH adjustment, the sequence of precipitate masses, from highest to lowest, was: 20 % $Ca(OH)_2$ > 20 % Na_2CO_3 > BAM-B > BAM-C > BAM-A > 40 % NaOH. This ordering indicates that while the three types of BAM produced a smaller precipitate mass relative to 20 % $Ca(OH)_2$ and 20 % Na_2CO_3, their effectiveness exceeded that of 40 % NaOH. Among the BAM types, BAM-A produced the least precipitate, with a difference of approximately 0.3 g from BAM-B and BAM-C. This variation is likely due to a lower quantity or absence of $Fe(NH_4)_2(SO_4)_2{\cdot}6\,H_2O$ precipitated during the treatment with BAM-A, a finding substantiated by Fig. 3 and reflected in BAM-A's

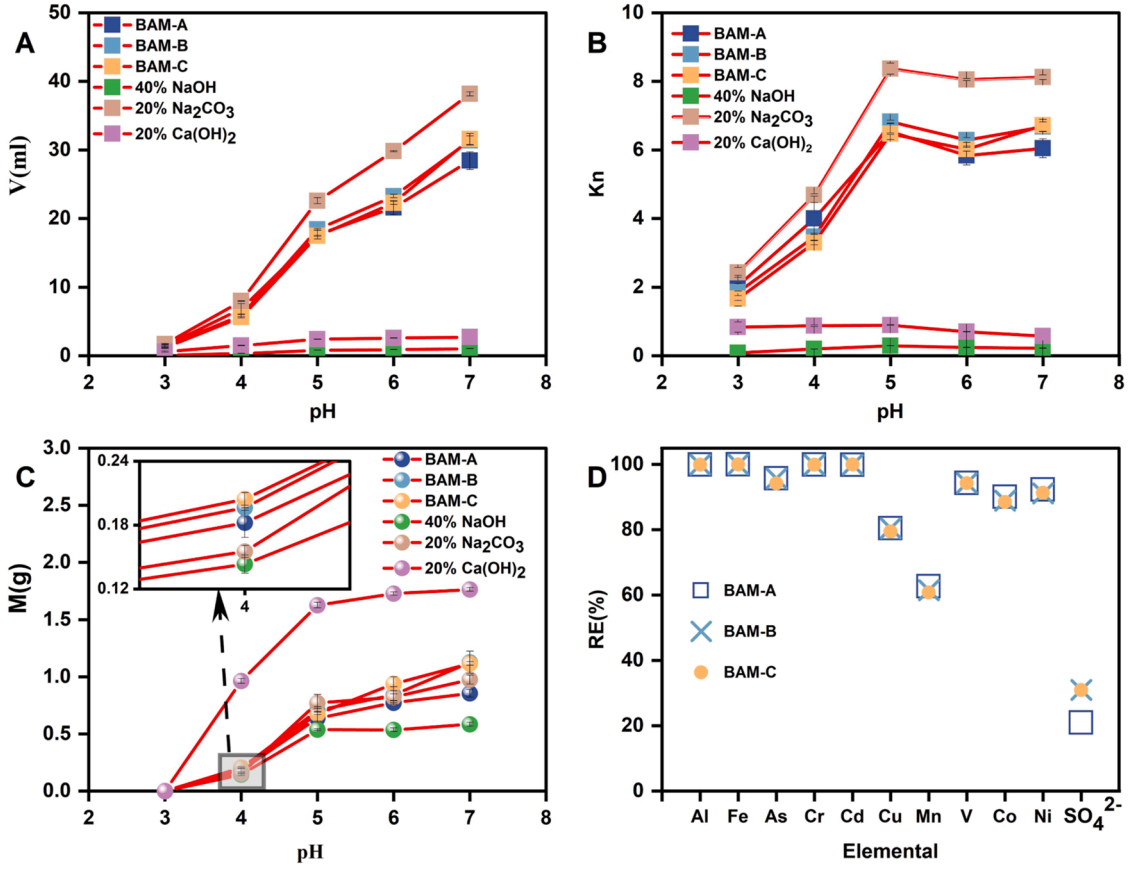

Fig. 5. Comparative analysis of reagent efficiency and outcome in AMD treatment. A shows the volumes of different reagents required to adjust the pH of AMD to specific values, showing each reagent's consumption rate. B shows the neutralization efficiency of these reagents, with smaller Kn values indicating higher effectiveness. C shows a variation curve for the mass of precipitates produced by the reagents at various pH levels. D shows the removal rates of metals and SO_4^{2-} achieved by three types of BAM when treating AMD to a target pH of 7.

lower SO_4^{2-} removal efficiency compared to BAM-B and BAM-C, as detailed in Fig. 5D. During the adjustment of AMD pH from 5 to 7 using alkaline reagents, the precipitate mass from 20 % Na_2CO_3 titration consistently increased, possibly due to induced carbonate formation (García-Valero et al., 2020).

Fig. 5D illustrates the metal removal efficiencies and SO_4^{2-} removal rates for three types of BAM when treating AMD to pH 7. The patterns of metal removal rates by the three BAM types are consistent. The removal rates for Al, Fe, Cr, and Cd are approximately 100 %, while As, V, Co, and Ni show removal rates between 90 % and 95 %. Cu and Mn have removal rates of 79—80 % and 60—62 %, respectively. It is noteworthy that the removal efficiency of Mn was significantly lower than that of other metals, which may be attributed to a combination of its coordination properties and relatively high initial concentration. On one hand, as a moderately hard acid, Mn tends to preferentially bind with medium-to-strong hard base ligands such as -OH and -COOH, while exhibiting weaker affinity toward $-NH_2$ groups, which are abundant in the BAM system. This results in a relative deficiency of effective coordination sites (Wang et al., 2020; Xu et al., 2017b). On the other hand, the initial concentration of Mn in AMD reached as high as 77.55 mg/L, substantially higher than that of Cd or Cr, thereby increasing competitive binding pressure and further limiting its removal efficiency. To improve Mn removal, strategies such as promoting MnS precipitation via SRB (sulfate-reducing bacteria)-mediated sulfate reduction, or enhancing complexation through recirculation to increase contact between Mn and ligands in BAM, may be considered (Bagheri Novair et al., 2024). At pH 7, the SO_4^{2-} removal rates are 21 % for BAM-A and 31 %—32 % for BAM-B and BAM-C. The variation in removal rates is mainly attributed to the precipitation of $Fe(NH_4)_2(SO_4)_2{\cdot}6\,H_2O$ during the treatment with BAM-B/C, which incorporates a portion of SO_4^{2-} into the precipitate. However, these removal rates do not meet the discharge limits set by various regions, necessitating further treatment for SO_4^{2-} (Chatla et al., 2023). Studies suggest that the presence of significant amounts of Fe and Al does not lead to the co-precipitation and substantial removal of Co, Ni, and Mn (Markovic et al., 2020; Seo et al., 2017), and adjusting the pH to 8–11 can enhance their removal (Klimko et al., 2023). Mn and Cd begin to precipitate as hydroxides at a pH exceeding 8 (Lewis, 2010). In this study, Co, Ni, Cd, and Mn exhibited high removal rates at pH 7, presumably due to the chelation of metal ions by the active functional groups in BAM. Additionally, V typically exists as metal oxide ions in wastewater, thus its removal through pH adjustment is generally ineffective; it is presumed to be removed via chelation as well (J. Liu et al., 2022).

The BAM–AMD step rapidly neutralises acidity and precipitates metals, but it also releases ca. 10 g/L NH_4^+ together with readily biodegradable metabolites such as ethanolamines, amides, glycerol and short-chain acids. Because these compounds are low-molecular-weight and labile, they are readily consumed in the biological "polishing" units that are routinely installed at AMD sites to meet tight NH_4^+, SO_4^{2-} and COD discharge limits. Typical options include sulfate-reducing-bacteria (SRB) reactors, Feammox-SRB coupled systems, up-flow anaerobic sludge blanket (UASB) units and constructed wetlands, which simultaneously convert SO_4^{2-} to innocuous sulfide while oxidising or assimilating NH_4^+ and residual organics (Wang et al., 2024b; Wimalaweera et al., 2025; Yan et al., 2022). The organic load introduced by BAM is modest relative to that from mine-camp sewage or flotation reagents often co-present in drainage, and thus it functions as an auxiliary electron donor rather than an added pollutant, completing a closed, multi-barrier remediation train.

Together, these results indicate several pathways for removing metals from AMD. Metal chelation can effectively remove Cr, Co, Ni, As, Cu, Mn, Cd, and V (Hossain et al., 2015; Padilla-Rodríguez et al., 2015; Rahman et al., 2023; Vaghetti et al., 2009). Co-precipitation can effectively target As and V (J. Liu et al., 2022; Yuan et al., 2021), and the co-precipitation with schwertmannite can also assist in

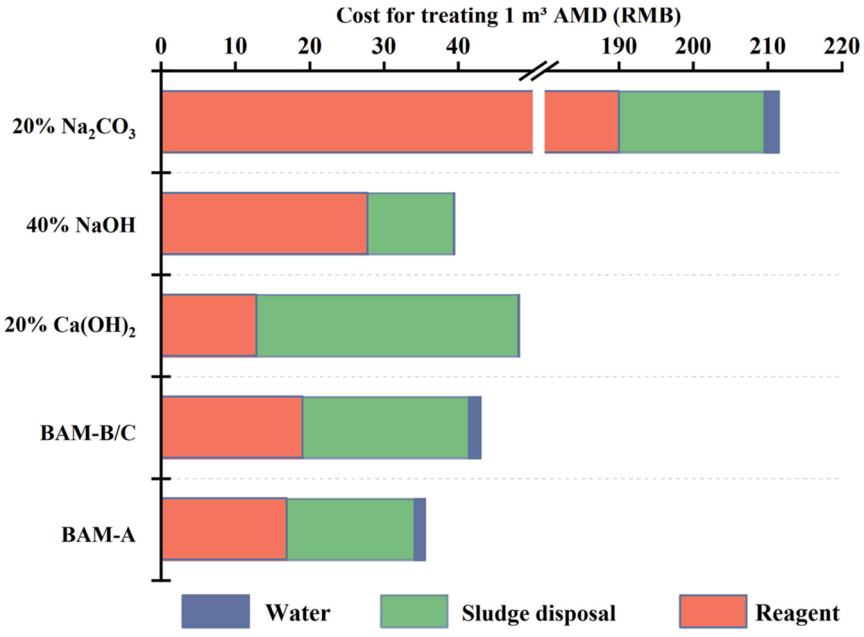

Fig. 6. Comparative costs analysis for treating one cubic meter of AMD, including reagent costs, sludge disposal costs, and water costs.

the removal of As and Cr (Xiong et al., 2023). The formation of hydroxides can facilitate the removal of Fe (II, III), Al (III), and Cu (II). Overall, BAM demonstrated a strong capacity to neutralize AMD pH and remove metals effectively.

3.6. Comprehensive cost analysis of reagents for AMD neutralization treatment

To evaluate the effectiveness and economic efficiency of various reagents in neutralizing AMD to pH = 7. We conducted a detailed cost analysis in Fig. 6, comparing their associated costs in terms of reagents, sludge disposal, and industrial water usage. The costs were calculated for treating 1 cubic meter of AMD, taking into account the disposal of hazardous waste sludge and the water costs associated with each treatment.

Fig. 6 presents a comparative analysis of the comprehensive costs associated with treating 1 m^3 of AMD. The costs range from the lowest to the highest as follows: BAM-A at 35.512 RMB/m^3, 40 % NaOH at 39.44 RMB/m^3, BAM-B/C at 43.006 RMB/m^3, 20 % Ca$(OH)_2$ at 48.187 RMB/m^3, and 20 % Na_2CO_3 at 211.510 RMB/m^3 . Water costs contribute minimally to the overall expenses, indicating that the major cost drivers are the reagents and sludge disposal. Notably, the cost of treating 1 m^3 AMD with 20 % Na_2CO_3 is several times higher than the other treatments, primarily due to its significant reagent expenses, rendering it economically unfavorable. The most cost-effective treatment for 1 m^3 AMD is BAM-A, despite producing more precipitate than 40 % NaOH when adjusting 100 mL AMD to pH= 7, suggesting an increase in sludge disposal costs. However, the lower cost of BAM-A reagents offsets these additional expenses, making it more economical overall compared to 40 % NaOH. Conversely, the overall cost for BAM-B/C variants is slightly higher than that of 40 % NaOH due to doubled sludge disposal costs, which negate the cost benefits from lower reagent expenses, resulting in a higher total cost for BAM-B/C. It is noteworthy that the reagent cost for treating 1 m^3 AMD with 20 % $Ca(OH)_2$ is the lowest among the treatments. However, the corresponding sludge disposal cost is two to three times higher than that of the other formulations, thereby diminishing the financial advantage gained from lower reagent costs. Variability in total costs across the three BAM treatments primarily arises from differences in sludge disposal costs, with BAM-B/C having a slightly higher reagent cost than BAM-A, but similar water costs.

In fact, the substantial discharges of acid mine wastewater, totaling 3.6 billion tons annually in China (Wang et al., 2024a) and approximately 400,000 megaliters in the Western region of South Africa (Masindi et al., 2022), emphasize the need for cost-effective AMD management solutions. In evaluating costs for large-scale AMD treatment, selecting the optimal reagent can lead to significant economic and environmental benefits. For an annual treatment volume of one million cubic meters, comprehensive costs escalate dramatically. Among the evaluated reagents, BAM-A offers notable savings: 12 million RMB compared to 20 % $Ca(OH)_2$, 3.5 million RMB relative to 40 % NaOH, and 174.5 million RMB versus 20 % Na_2CO_3. The benefits of using BAM-A grow with treatment volume, enhancing its suitability for long-term mining operations and potentially reducing overall costs through water recycling. Moreover, scaling factors significantly impact cost efficiency as treatment volumes increase. Costs associated with BAM production are likely to decrease due to economies of scale. This is typical for biological systems where larger volumes lead to more efficient resource use and lower per-unit costs, driven by initial setup and culture development. Conversely, the costs for chemical reagents such as $Ca(OH)_2$, NaOH, and Na_2CO_3 may increase with scale. While bulk purchasing might reduce material costs, handling and application expenses, especially those related to safety and infrastructure needs due to the corrosive nature of these chemicals, are likely to rise. Additionally, the need for complex mixing and control systems at larger scales could further inflate costs. Thus, the savings using BAM can be considerably greater, especially when factored over the long term and across large volumes, underscoring its economic and environmental viability for AMD treatment projects.

Operational implications reveals that for achieving pH 7, 40 % NaOH requires additional quantities for effective metal removal, leading to higher downstream acid reduction treatments and associated costs. NaOH, a potent alkaline with considerable energy demands, also incurs elevated storage and handling expenses (Kennedy and Arias-Paić, 2020). In contrast, BAM, a milder alkaline, reduces operational costs due to less stringent storage requirements. The use of $Ca(OH)_2$ often necessitates excessive amounts to achieve treatment goals, elevating water hardness and necessitating further softening and acid treatments, thereby increasing operational expenses. Furthermore, the traditional application of $Ca(OH)_2$ in AMD treatment can result in blockages and additional costs due to the formation of surface layers on the $Ca(OH)_2$ particles (Song et al., 2022). Optimizing BAM formulations to decrease urea content may further reduce reagent costs. Consequently, BAM, especially BAM-A, presents a significant reduction in operational costs and stands out as a practical option for AMD treatment, with substantial economic and environmental advantages.

Taken together, the foregoing results confirm that BAM is technically feasible and economically attractive for AMD treatment. Yet to appreciate the full significance of these findings, it is essential to view them against the backdrop of what the AMD-remediation literature still lacks: (i) Limited studies have benchmarked bio-alkali fluids against the complete set of conventional bases under strictly identical AMD conditions; our side-by-side titrations close that gap. (ii) The dual mechanism in which BAM couples alkaline buffering with ligand-driven metal chelation has remained speculative; by linking identified functional groups in BAM to both removal efficiencies and precipitate mineralogy, we provide the first experimental verification. (iii) precipitate speciation during BAM neutralisation, especially the coexistence of Fe/Al hydroxysulfates and organo-metal complexes, was unclear; XRD and geochemical profiling here clarify this pathway. (iv) The holistic techno-economic assessment of BAM at scale is important for its application; our cost model supplies that critical benchmark. By filling these research gaps, the present work reframes BAM as a mechanistically understood and commercially viable alternative for sustainable AMD remediation.

4. Conclusion

In this study, we have demonstrated that the BAM formulations, particularly BAM-A, significantly enhance the removal of heavy

metals from AMD when adjusted to a pH of 7. The three strains of bacteria isolated, *Pseudogracilibacillus* from UPMC-A, *Pseudochrobactrum* from UPMC-B, and *Myroides* from UPMC-C, proved adept at thriving in environments with weak alkalinity and high ammonia concentrations, which is critical for the sustainability of bioremediation processes in AMD treatments. The organic components identified in BAM, containing functional groups like -$CONH_2$, -NH_2, -OH, and -COOH, and particularly the presence of alkaloids in BAM-A, are instrumental in the successful neutralization and metal remediation processes.

Our results confirm that the unique bio-alkaline mixture of BAM when used in a ratio of 3:10 with AMD, not only brings the pH down to neutral but also effectively precipitates out metals such as Aluminum, Iron, Chromium, and Cadmium nearly completely, and achieves substantial removal of As, V, Co, Ni, and Cu. However, the removal rates for Manganese and Sulfates, although significant, did not meet the discharge standards, highlighting areas for future improvement. The efficacy in managing metal concentrations in AMD suggests that the application of BAM could be significantly cost-effective, with BAM-A showing the most promise in reducing operational costs.

The findings from this study provide a foundation for further research, particularly in optimizing the treatment process to enhance the removal rates of less responsive contaminants like Manganese. Future experiments could explore the modification of effluent recirculation ratios to achieve this. Overall, our study underscores the potential of BAM, especially BAM-A, as a viable and economically advantageous solution for the treatment of AMD, offering substantial environmental benefits and aligning with sustainable mining practices. This contribution is poised to influence future strategies in AMD management, focusing on improving cost-efficiency and compliance with environmental standards.

CRediT authorship contribution statement

Cong Peng: Writing – original draft, Visualization, Validation, Methodology, Investigation, Conceptualization. **Li Zeng:** Writing – review & editing, Resources, Project administration, Methodology. **Yonghong Liu:** Writing – review & editing, Resources, Data curation. **Zhenyu Zhang:** Visualization, Investigation, Data curation. **Jiayi Tang:** Visualization, Investigation, Data curation. **Zhenghua Liu:** Writing – review & editing. **Zhaoyue Yang:** Investigation, Formal analysis. **Huaqun Yin:** Writing – original draft, Validation. **I.A. Ibrahim:** Writing – review & editing. **Ke Zhang:** Data curation. **Zhendong Yang:** Writing – review & editing, Writing – original draft, Validation, Supervision, Project administration, Methodology, Funding acquisition, Formal analysis, Data curation, Conceptualization.

Declaration of Competing Interest

The authors declare that they have no known competing financial interests or personal relationships that could have appeared to influence the work reported in this paper.

Acknowledgment

This work was funded by the National Key Research and Development Program of China (2023YFE0114500); Natural Science Foundation of Sichuan (2023NSFSC0845); Sichuan Provincial Engineering Research Center of City Solid Waste Energy and Building Materials Conversion and Utilization Technology (GF2024ZC07).

Data availability

Data will be made available on request.

References

Alizadeh, H., Kandula, D.R.W., Hampton, J.G., Stewart, A., Leung, D.W.M., Edwards, Y., Smith, C., 2017. Urease producing microorganisms under dairy pasture management in soils across New Zealand. Geoderma Reg. 11, 78–85. https://doi.org/10.1016/j.geodrs.2017.10.003.

Bagheri Novair, S., Biglari, Z., Asgari Lajayer, B., Shu, W., Price, G.W., 2024. The role of sulphate-reducing bacteria (SRB) in bioremediation of sulphate-rich wastewater: focus on the source of electron donors. Process Saf. Environ. Prot. 184, 190–207. https://doi.org/10.1016/j.psep.2024.01.103.

Biswas, S., Biswas, R., 2023. Chitosan-the miracle biomaterial as detection and diminishing mediating agent for heavy metal ions: a mini review. Chemosphere 312 (Pt 1), 137187. https://doi.org/10.1016/j.chemosphere.2022.137187.

Carneiro Brandão Pereira, T., Batista dos Santos, K., Lautert-Dutra, W., de Souza Teodoro, L., de Almeida, V.O., Weiler, J., Homrich Schneider, I.A., Reis Bogo, M., 2020. Acid mine drainage (AMD) treatment by neutralization: evaluation of physical-chemical performance and ecotoxicological effects on zebrafish (Danio rerio) development. Chemosphere 253, 126665. https://doi.org/10.1016/j.chemosphere.2020.126665.

Chatla, A., Almanassra, I.W., Abushawish, A., Laoui, T., Alawadhi, H., Atieh, M.A., Ghaffour, N., 2023. Sulphate removal from aqueous solutions: state-of-the-art technologies and future research trends. Desalination 558. https://doi.org/10.1016/j.desal.2023.116615.

Diez-Marulanda, J.C., Brandao, P.F.B., 2023. Isolation of urease-producing bacteria from cocoa farms soils in Santander, Colombia, for cadmium remediation. 3 Biotech 13 (3), 98. https://doi.org/10.1007/s13205-023-03495-1.

Ding, B., Wang, X., Feng, K., Fu, J., Liang, J., Zhou, L., 2022. Efficient adsorption of Cr(VI) in acidic environment by nano-scaled schwertmannite prepared through pH regulation: characteristics, performances, and mechanism. Environ. Sci. Pollut. Res. Int. 29 (51), 77344–77358. https://doi.org/10.1007/s11356-022-21257-z.

Dubey, A.A., Ravi, K., Mukherjee, A., Sahoo, L., Abiala, M.A., Dhami, N.K., 2021. Biocementation mediated by native microbes from Brahmaputra riverbank for mitigation of soil erodibility. Sci. Rep. 11 (1), 15250. https://doi.org/10.1038/s41598-021-94614-6.

Elmi, F., Etemadifar, Z., Emtiazi, G., 2022. Calcite nanocrystal production using locally isolated ureolytic bacteria and assessing their resistance to extreme conditions. Iran. J. Sci. Technol. Trans. A: Sci. 46 (6), 1523–1530. https://doi.org/10.1007/s40995-022-01366-7.

Emik, S., 2014. Preparation and characterization of an IPN type chelating resin containing amino and carboxyl groups for removal of Cu(II) from aqueous solutions. React. Funct. Polym. 75, 63–74. https://doi.org/10.1016/j.reactfunctpolym.2013.12.006.

Esteban-Gutiérrez, M., Garcia-Aguirre, J., Irizar, I., Aymerich, E., 2018. From sewage sludge and agri-food waste to VFA: individual acid production potential and up-scaling. Waste Manag. 77, 203–212. https://doi.org/10.1016/j.wasman.2018.05.027.
Fan, Y.J., Hu, X.M., Zhao, Y.Y., Wu, M.Y., Wang, S.M., Wang, P.Y., Xue, Y., Zhu, S.C., 2020. Urease producing microorganisms for coal dust suppression isolated from coal: characterization and comparative study [Article]. Adv. Powder Technol. 31 (9), 4095–4106. https://doi.org/10.1016/j.apt.2020.08.014.
García-Valero, A., Martínez-Martínez, S., Faz, A., Rivera, J., Acosta, J.A., 2020. Environmentally sustainable acid mine drainage remediation: use of natural alkaline material. J. Water Process Eng. 33. https://doi.org/10.1016/j.jwpe.2019.101064.
Ghezelbash, G.R., Haddadi, M., 2018. Production of nanocalcite crystal by a urease producing halophilic strain of Staphylococcus saprophyticus and analysis of its properties by XRD and SEM. World J. Microbiol. Biotechnol. 34 (12), 174. https://doi.org/10.1007/s11274-018-2544-2.
Goldford, J.E., Lu, N., Bajić, D., Estrela, S., Tikhonov, M., Sanchez-Gorostiaga, A., Segrè, D., Mehta, P., Sanchez, A., 2018. Emergent simplicity in microbial community assembly. Science 361 (6401), 469–474. https://doi.org/10.1126/science.aat1168.
Gupta, S., Thapliyal, P., Shah, V., Daverey, A., 2022. Optimization of bio-calcification process for a newly isolated urease producing bacterial strain Advenelle sp. AV1. Geomicrobiol. J. 39 (3-5), 242–248. https://doi.org/10.1080/01490451.2021.1980920.
Hamzah, A., Phan, C.-W., Abu Bakar, N.F., Wong, K.-K., 2013. Biodegradation of crude oil by constructed bacterial consortia and the constituent single bacteria isolated From Malaysia. Bioremediation J. 17 (1), 1–10. https://doi.org/10.1080/10889868.2012.731447.
He, X., Wang, H., Tang, C., Yan, H., Jin, H., 2024. Potassium-bicarbonate-induced mineralized acid mine drainage into iron hydroxyl sulfate minerals for better water remediation and resource reuse. Sustainability 16 (2). https://doi.org/10.3390/su16020554.
Heidari Nonakaran, S., Pazhouhandeh, M., Keyvani, A., Abdollahipour, F.Z., Shirzad, A., 2015. Isolation and identification of Pseudomonas azotoformans for induced calcite precipitation. World J. Microbiol. Biotechnol. 31 (12), 1993–2001. https://doi.org/10.1007/s11274-015-1948-5.
Hossain, A., Bhattacharyya, S.R., Aditya, G., 2015. Biosorption of cadmium from aqueous solution by shell dust of the freshwater snail Lymnaea luteola. Environ. Technol. Innov. 4, 82–91. https://doi.org/10.1016/j.eti.2015.05.001.
Jalilvand, N., Akhgar, A., Alikhani, H.A., Rahmani, H.A., Rejali, F., 2019. Removal of heavy metals zinc, lead, and cadmium by biomineralization of urease-producing bacteria isolated from iranian mine calcareous soils. J. Soil Sci. Plant Nutr. 20 (1), 206–219. https://doi.org/10.1007/s42729-019-00121-z.
Jia, L., Liu, H., Kong, Q., Li, M., Wu, S., Wu, H., 2020. Interactions of high-rate nitrate reduction and heavy metal mitigation in iron-carbon-based constructed wetlands for purifying contaminated groundwater. Water Res. 169, 115285. https://doi.org/10.1016/j.watres.2019.115285.
Jiang, W., Yang, Y., Miao, S., Wan, D., 2023. Fabrication of a novel chitosan/polyaspartic acid composite: a pH-tunable sorbent for efficient adsorption of heavy metal ions and dyes from water. J. Water Process Eng. 56. https://doi.org/10.1016/j.jwpe.2023.104554.
Jiang, N.-J., Yoshioka, H., Yamamoto, K., Soga, K., 2016. Ureolytic activities of a urease-producing bacterium and purified urease enzyme in the anoxic condition: implication for subseafloor sand production control by microbially induced carbonate precipitation (MICP). Ecol. Eng. 90, 96–104. https://doi.org/10.1016/j.ecoleng.2016.01.073.
Jiao, Y., Zhang, C., Su, P., Tang, Y., Huang, Z., Ma, T., 2023. A review of acid mine drainage: formation mechanism, treatment technology, typical engineering cases and resource utilization. Process Saf. Environ. Prot. 170, 1240–1260. https://doi.org/10.1016/j.psep.2022.12.083.
Johnston, S.G., Burton, E.D., Moon, E.M., 2016. Arsenic mobilization is enhanced by thermal transformation of schwertmannite. Environ. Sci. Technol. 50 (15), 8010–8019. https://doi.org/10.1021/acs.est.6b02618.
Kanmani, P., Aravind, J., Kamaraj, M., Sureshbabu, P., Karthikeyan, S., 2017. Environmental applications of chitosan and cellulosic biopolymers: a comprehensive outlook [Review]. Bioresour. Technol. 242, 295–303. https://doi.org/10.1016/j.biortech.2017.03.119.
Kennedy, A.M., Arias-Paić, M., 2020. Application of powdered steel slag for more sustainable removal of metals from impaired waters. J. Water Process Eng. 38, 101599. https://doi.org/10.1016/j.jwpe.2020.101599.
Khadim, H.J., Ammar, S.H., Ebrahim, S.E., 2019. Biomineralization based remediation of cadmium and nickel contaminated wastewater by ureolytic bacteria isolated from barn horses soil. Environ. Technol. Innov. 14. https://doi.org/10.1016/j.eti.2019.100315.
Klimko, J., Takacova, Z., Marcinov, V., Piroskova, J., Vindt, T., Liptai, P., Orac, D., 2023. Lithium slag leach solution refining by hydroxide precipitation. J. Min. Metall. Sect. B Metall. https://doi.org/10.2298/JMMB231020042K 42-42.
Koskue, V., Pyrhönen, V.-P., Freguia, S., Ledezma, P., Kokko, M., 2022. Modelling and techno-economic assessment of (bio)electrochemical nitrogen removal and recovery from reject water at full WWTP scale. J. Environ. Manag. 319, 115747. https://doi.org/10.1016/j.jenvman.2022.115747.
Lewis, A.E., 2010. Review of metal sulphide precipitation. Hydrometallurgy 104 (2), 222–234. https://doi.org/10.1016/j.hydromet.2010.06.010.
Li, Q., Zhang, W., 2022. Process development for recovering critical elements from acid mine drainage. Resour. Conserv. Recycl. 180, 106214. https://doi.org/10.1016/j.resconrec.2022.106214.
Liu, J., Huang, Y., Li, H., Duan, H., 2022. Recent advances in removal techniques of vanadium from water: a comprehensive review. Chemosphere 287 (Pt 1), 132021. https://doi.org/10.1016/j.chemosphere.2021.132021.
Liu, W.H., Zhao, Y.Y., Hu, X.M., Li, X., Geng, Z., Wang, Q.S., Liu, J.D., Wang, H.Y., You, G.Y., 2022. High performance of coal dust suppression with waste activated sludge using microbially induced calcite precipitation technology. Powder Technol. 404 (10), 117464. https://doi.org/10.1016/j.powtec.2022.117464.
Liu, Z.X., Zhuang, J.Y., Liu, C., Zheng, K., Chen, L., 2023. Analysis of soil bacterial community structure and ecological function characteristics in different pollution levels of lead-zinc tailings in Datong. Huan Jing Ke Xue 44 (7), 4191–4200. https://doi.org/10.13227/j.hjkx.202209160.
Lopez, J., Reig, M., Gibert, O., Valderrama, C., Cortina, J.L., 2018. Evaluation of NF membranes as treatment technology of acid mine drainage: metals and sulfate removal. Desalination 440, 122–134. https://doi.org/10.1016/j.desal.2018.03.030.
Lottermoser, B., 2015. Predicting acid mine drainage: past, present, future. Gl. ückauf Min. Rep. 151, 480–489.
Lu, Y.Q., Fan, L.H., Yang, L.Y., Huang, F.F., Ouyang, X.K., 2020. PEI-modified core-shell/bead-like amino silica enhanced poly (vinyl alcohol)/chitosan for diclofenac sodium efficient adsorption [Article]. Carbohydr. Polym. 229 (11), 115459. https://doi.org/10.1016/j.carbpol.2019.115459.
Ma, L., Pang, A.-P., Luo, Y., Lu, X., Lin, F., 2020. Beneficial factors for biomineralization by ureolytic bacterium Sporosarcina pasteurii. Microb. Cell Factor. 19 (1), 12. https://doi.org/10.1186/s12934-020-1281-z.
Mao, Z., Yu, C., Xin, L., 2015. Enhancement of phenol biodegradation by Pseudochrobactrum sp. through ultraviolet-induced mutation. Int. J. Mol. Sci. 16 (4), 7320–7333. https://doi.org/10.3390/ijms16047320.
Marín, S., Cabestrero, O., Demergasso, C., Olivares, S., Zetola, V., Vera, M., 2021. An indigenous bacterium with enhanced performance of microbially-induced Ca-carbonate biomineralization under extreme alkaline conditions for concrete and soil-improvement industries [Article]. Acta Biomater. 120, 304–317. https://doi.org/10.1016/j.actbio.2020.11.016.
Markovic, R., Bessho, M., Masuda, N., Stevanovic, Z., Bozic, D., Apostolovski Trujic, T., Gardic, V., 2020. New approach of metals removal from acid mine drainage. Appl. Sci. 10 (17). https://doi.org/10.3390/app10175925.
Masindi, V., Foteinis, S., Renforth, P., Ndiritu, J., Maree, J.P., Tekere, M., Chatzisymeon, E., 2022. Challenges and avenues for acid mine drainage treatment, beneficiation, and valorisation in circular economy: a review. Ecol. Eng. 183. https://doi.org/10.1016/j.ecoleng.2022.106740.
Mei, Y., Zhuang, S., Wang, J., 2025. Adsorption of heavy metals by biochar in aqueous solution: a review. Sci. Total Environ. 968, 178898. https://doi.org/10.1016/j.scitotenv.2025.178898.
Mempin1, R., H. T., C. C., H. G., &, K. K. H. a. S. L., 2013. Release of extracellular ATP by bacteria during growth. BMC Microbiol. https://doi.org/10.1186/1471-2180-13-301.
Newton, K., Gonzalez, E., Pitre, F.E., Brereton, N.J.B., 2022. Microbial community origin and fate through a rural wastewater treatment plant. Environ. Microbiol. 24 (5), 2516–2542. https://doi.org/10.1111/1462-2920.16025.
Ospina-Betancourth, C., Acharya, K., Allen, B., Entwistle, J., Head, I.M., Sanabria, J., Curtis, T.P., 2020. Enrichment of nitrogen-fixing bacteria in a nitrogen-deficient wastewater treatment system [Article]. Environ. Sci. Technol. 54 (6), 3539–3548. https://doi.org/10.1021/acs.est.9b05322.
Otunola, B.O., Mhangara, P., 2024. Global advancements in the management and treatment of acid mine drainage. Appl. Water Sci. 14 (9), 204. https://doi.org/10.1007/s13201-024-02259-3.

Padilla-Rodríguez, A., Hernández-Viezcas, J.A., Peralta-Videa, J.R., Gardea-Torresdey, J.L., Perales-Pérez, O., Román-Velázquez, F.R., 2015. Synthesis of protonated chitosan flakes for the removal of vanadium(III, IV and V) oxyanions from aqueous solutions. Microchem. J. 118, 1–11. https://doi.org/10.1016/j.microc.2014.07.011.

Paikaray, S., 2021. Environmental stability of schwertmannite: a review. Mine Water Environ. 40 (3), 570–586. https://doi.org/10.1007/s10230-020-00734-2.

Palakodeti, A., Azman, S., Rossi, B., Dewil, R., Appels, L., 2021. A critical review of ammonia recovery from anaerobic digestate of organic wastes via stripping. Renew. Sustain. Energy Rev. 143 (14), 110903. https://doi.org/10.1016/j.rser.2021.110903.

Pang, G., Cai, F., Li, R.X., Zhao, Z., Li, R., Gu, X.L., Shen, Q.R., Chen, W., 2017. Trichoderma-enriched organic fertilizer can mitigate microbiome degeneration of monocropped soil to maintain better plant growth. Plant Soil 416 (1-2), 181–192. https://doi.org/10.1007/s11104-017-3178-0.

Qin, J., Qin, Q., Li, X., Xue, J., Wang, R., Zhang, Q., Wang, P., Guo, Z., Gong, Y., 2021. Urea supply control in microbial carbonate precipitation to effectively fill pores of concrete. Constr. Build. Mater. 310, 125123. https://doi.org/10.1016/j.conbuildmat.2021.125123.

Qiu, S., Qiu, T., Yan, H., Long, Q., Wu, H., Li, X., Zhu, D., 2022. Investigation of protonation and deprotonation processes of kaolinite and its effect on the adsorption stability of rare earth elements. Colloids Surf. A: Physicochem. Eng. Asp. 642. https://doi.org/10.1016/j.colsurfa.2022.128596.

Rahman, A., Haque, M.A., Ghosh, S., Shinu, P., Attimarad, M., Kobayashi, G., 2023. Modified shrimp-based chitosan as an emerging adsorbent removing heavy metals (Chromium, Nickel, Arsenic, and Cobalt) from polluted water. Sustainability 15 (3). https://doi.org/10.3390/su15032431.

Rezaie, B., Anderson, A., 2020. Sustainable resolutions for environmental threat of the acid mine drainage. Sci. Total Environ. 717, 137211. https://doi.org/10.1016/j.scitotenv.2020.137211.

Rose, C., Parker, A., Jefferson, B., Cartmell, E., 2015. The Characterization of feces and urine: a review of the literature to inform advanced treatment technology. Crit. Rev. Environ. Sci. Technol. 45 (17), 1827–1879. https://doi.org/10.1080/10643389.2014.1000761.

Ruacho, A., Richon, C., Whitby, H., Bundy, R.M., 2022. Sources, sinks, and cycling of dissolved organic copper binding ligands in the ocean. Commun. Earth Environ. 3 (1), 263. https://doi.org/10.1038/s43247-022-00597-1.

Sander, R., 2015. Compilation of Henry's law constants (version 4.0) for water as solvent. Atmos. Chem. Phys. 15 (8), 4399–4981. https://doi.org/10.5194/acp-15-4399-2015.

Seo, E.Y., Cheong, Y.W., Yim, G.J., Min, K.W., Geroni, J.N., 2017. Recovery of Fe, Al and Mn in acid coal mine drainage by sequential selective precipitation with control of pH. Catena 148, 11–16. https://doi.org/10.1016/j.catena.2016.07.022.

Shi, W., Dong, Q., Saleem, M., Wu, X., Wang, N., Ding, S., Huang, J., Wang, X., Zhou, B., Gao, Z., 2022. Microbial-based detonation and processing of vegetable waste for high quality compost production at low temperatures. J. Clean. Prod. 369, 133276. https://doi.org/10.1016/j.jclepro.2022.133276.

Song, Y., Guo, Z., Wang, R., Yang, L., Cao, Y., Wang, H., 2022. A novel approach for treating acid mine drainage by forming schwertmannite driven by a combination of biooxidation and electroreduction before lime neutralization. Water Res. 221, 118748. https://doi.org/10.1016/j.watres.2022.118748.

Sun, Y., Zhou, S., Pan, S.-Y., Zhu, S., Yu, Y., Zheng, H., 2020. Performance evaluation and optimization of flocculation process for removing heavy metal. Chem. Eng. J. 385, 123911. https://doi.org/10.1016/j.cej.2019.123911.

Thomas, F., Hehemann, J.H., Rebuffet, E., Czjzek, M., Michel, G., 2011. Environmental and gut bacteroidetes: the food connection. Front Microbiol. 2, 93. https://doi.org/10.3389/fmicb.2011.00093.

Toby, B.H., 2006. R factors in Rietveld analysis: how good is good enough? Powder Diffr. 21 (1), 67–70. https://doi.org/10.1154/1.2179804.

Turingan, C.O.A., Lintag, N.E.S., Ngan, C.I.L., Soriano, E.J.D., Orbecido, A.H., 2021. Post-treatment of acid mine drainage using laboratory-extracted common mushroom chitosan. Chem. Eng. Technol. 44 (11), 1962–1969. https://doi.org/10.1002/ceat.202100220.

Vaghetti, J.C.P., Lima, E.C., Royer, B., da Cunha, B.M., Cardoso, N.F., Brasil, J.L., Dias, S.L.P., 2009. Pecan nutshell as biosorbent to remove Cu(II), Mn(II) and Pb(II) from aqueous solutions. J. Hazard. Mater. 162 (1), 270–280. https://doi.org/10.1016/j.jhazmat.2008.05.039.

Wang, Y., Cao, J., Biswas, A., Fang, W., Chen, L., 2024a. Acid mine wastewater treatment: a scientometrics review. J. Water Process Eng. 57, 104713. https://doi.org/10.1016/j.jwpe.2023.104713.

Wang, S., Cao, J., Jia, W., Guo, W., Yan, S., Wang, Y., Zhang, P., Chen, H.-Y., Huang, S., 2020. Single molecule observation of hard–soft-acid–base (HSAB) interaction in engineered Mycobacterium smegmatis porin A (MspA) nanopores††Electronic supplementary information (ESI) available. Chem. Sci. 11 (3), 879–887. https://doi.org/10.1039/c9sc05260g.

Wang, G., Li, B., Peng, D., Zhao, H., Lu, M., Zhang, L., Li, J., Zhang, S., Guan, C., Ji, J., 2022. Combined application of H2S and a plant growth promoting strain JIL321 regulates photosynthetic efficacy, soil enzyme activity and growth-promotion in rice under salt stress. Microbiol. Res. 256, 126943. https://doi.org/10.1016/j.micres.2021.126943.

Wang, B., Sun, D., Yuan, T.-Q., Song, G., Sun, R.-C., 2021. Recent advances in lignin modification and its application in wastewater treatment. 143-173. https://doi.org/10.1021/bk-2021-1377.ch007.

Wang, H., Zhang, M., Dong, P., Xue, J., Liu, L., 2024b. Bioremediation of acid mine drainage using sulfate-reducing wetland bioreactor: filling substrates influence, sulfide oxidation and microbial community. Chemosphere 349, 140789. https://doi.org/10.1016/j.chemosphere.2023.140789.

Williamson, A., Verbruggen, F., Chavez Rico, V.S., Bergmans, J., Spooren, J., Yurramendi, L., Du Laing, G., Boon, N., Hennebel, T., 2020. Selective leaching of copper and zinc from primary ores and secondary mineral residues using biogenic ammonia. J. Hazard. Mater. 403. https://doi.org/10.1016/j.jhazmat.2020.123842.

Wimalaweera, I., Zuo, F., Tang, Q., Sui, Q., Jinadasa, S., Weragoda, S., Ritigala, T., Weerasooriya, R., Wang, Y., Zhong, H., Makehelwala, M., Wei, Y., 2025. Synchronised removal of nitrogen and sulphate from rubber industrial wastewater by coupling of Sulfammox and sulphide-driven autotrophic denitrification in anaerobic membrane bioreactor. Bioresour. Technol. 416, 131785. https://doi.org/10.1016/j.biortech.2024.131785.

Xiong, H.X., Liu, Y., Wang, S.Y., Zhu, S.B., 2023. Schwertmannite and akaganeite for adsorption removals of Cr(VI) from aqueous solutions. Environ. Sci. Pollut. Res. 30 (22), 62295–62311. https://doi.org/10.1007/s11356-023-26348-z.

Xu, G., Li, D., Jiao, B., Li, D., Yin, Y., Lun, L., Zhao, Z., Li, S., 2017a. Biomineralization of a calcifying ureolytic bacterium Microbacterium sp. GM-1. Electron. J. Biotechnol. 25, 21–27. https://doi.org/10.1016/j.ejbt.2016.10.008.

Xu, H., Xu, D.C., Wang, Y., 2017b. Natural indices for the chemical hardness/softness of metal cations and ligands. ACS Omega 2 (10), 7185–7193. https://doi.org/10.1021/acsomega.7b01039.

Xuesong, H., Banghua, H., Yingchao, L., Suya, M., Caihong, Y., 2024. Genomic characterization of a novel ureolytic bacteria, Lysinibacillus capsici TSBLM, and its application to the remediation of acidic heavy metal-contaminated soil. Sci. Total Environ. 927, 172170. https://doi.org/10.1016/j.scitotenv.2024.172170.

Yan, J., Luo, F., Wu, l, Ou, Y., Gong, C., Hao, T., Huang, L., Chen, Y., Long, J., Xiao, T., Zhang, H., 2022. Cost-effective desulfurization of acid mine drainage with food waste as an external carbon source: a pilot-scale and long-term study. J. Clean. Prod. 361, 132174. https://doi.org/10.1016/j.jclepro.2022.132174.

Yang, Y., Chu, J., Cao, B., Liu, H.L., Cheng, L., 2020. Biocementation of soil using non-sterile enriched urease-producing bacteria from activated sludge. J. Clean. Prod. 262 (10), 121315. https://doi.org/10.1016/j.jclepro.2020.121315.

Yang, Y., Li, B., Che, L., Li, M., Liu, P., Li, T., Luo, Y., 2024. A review on 'source prevention, process control, end recovery' trinity-comprehensive treatment technology for acid mine drainage. Process Saf. Environ. Prot. 189, 782–801. https://doi.org/10.1016/j.psep.2024.06.125.

Yuan, Z., Ma, X., Wang, S., Yu, L., Zhang, P., Lin, J., Jia, Y., 2021. Effect of co-existent Al(III) in As-rich Acid Mine Drainage (AMD) on As removal during Fe(II) and As (III) abiotic oxidation process. J. Water Process Eng. 44, 102395. https://doi.org/10.1016/j.jwpe.2021.102395.

Yujing, L., Linghua, Z., Weifeng, L., Zepeng, Z., 2022. Simultaneous removal of urea nitrogen and inorganic nitrogen from high-salinity wastewater by Halomonas sp. H36. Environ. Sci. Pollut. Res. 30 (2), 2544–2554. https://doi.org/10.1007/s11356-022-22018-8.

Zhou, L., Gao, Y., Yu, K., Zhou, H., De Costa, Y.G., Yi, S., Zhuang, W.-Q., 2020. Microbial community in in-situ waste sludge anaerobic digestion with alkalization for enhancement of nutrient recovery and energy generation. Bioresour. Technol. 295, 122277. https://doi.org/10.1016/j.biortech.2019.122277.

Zhu, B.-K., Fang, Y.-M., Zhu, D., Christie, P., Ke, X., Zhu, Y.-G., 2018. Exposure to nanoplastics disturbs the gut microbiome in the soil oligochaete Enchytraeus crypticus. Environ. Pollut. 239, 408–415. https://doi.org/10.1016/j.envpol.2018.04.017.

ZvinowandaCaliphs, 2023. Recent development of active technologies for AMD treatment. Hybridized Technol. Treat. Min. Effl. 95–117. https://doi.org/10.1002/9781119896920.ch4.